The Meteoritical Society

Meteoritics & Planetary Science 58, Nr 11, 1580–1599 (2023)
doi: 10.1111/maps.14085

Light noble gases in 11 achondrites: Cosmic ray exposure ages, gas retention ages, and preatmospheric sizes

Thomas SMITH [1]*, Huaiyu HE [1,2,3]*, Shijie LI [4], and Fei SU [1]

[1]State Key Laboratory of Lithospheric Evolution, Institute of Geology and Geophysics, Chinese Academy of Sciences, Beijing, China
[2]Institutions of Earth Science, Chinese Academy of Sciences, Beijing, China
[3]College of Earth and Planetary Sciences, University of Chinese Academy of Sciences, Beijing, China
[4]Center for Lunar and Planetary Sciences, Institute of Geochemistry, Chinese Academy of Sciences, Guiyang, China
***Correspondence**
Thomas Smith and Huaiyu He, State Key Laboratory of Lithospheric Evolution, Institute of Geology and Geophysics, Chinese Academy of Sciences, Beijing 100029, China.
Email: thomas.smith@mail.iggcas.ac.cn; huaiyuhe@mail.iggcas.ac.cn

(Received 07 September 2022; revision accepted 31 July 2023)

Abstract–We report light noble gas (He, Ne, and Ar) concentrations and isotopic ratios in 11 achondrites, Tafassasset (unclassified primitive achondrite), Northwest Africa (NWA) 12934 (angrite), NWA 12573 (brachinite), Jiddat al Harasis (JaH) 809 (ureilite), NWA 11562 (ungrouped achondrite), four lodranites (NWA 11901, NWA 7474, NWA 6685, and NWA 6484), NWA 2871 (acapulcoite), and Sahara 02029 (winonaite), most of which have not been previously studied for noble gases. We discuss their noble gas isotopic composition, determine their cosmogenic nuclide content, and systematically calculate their cosmic ray exposure (CRE) and gas retention ages. In addition, we estimate their preatmospheric radii and preatmospheric masses based on the shielding parameter $(^{22}Ne/^{21}Ne)_{cos}$. None of the studied meteorites shows evidence of contribution from solar cosmic rays (SCRs). JaH 809 and NWA 12934 show evidence of ^{3}He diffusive losses of >90% and 40%, respectively. The winonaite Sahara 02029 has lost most of its noble gases, either during or before analysis. The average CRE age of Tafassasset of ~49 Ma is lower than that reported by Patzer et al. (2003), but is consistent with it within the uncertainties; this confirms that Tafassasset and CR chondrites are not source paired, CR chondrites having CRE ages from 1 to 25 Ma (Herzog & Caffee, 2014). The ureilite JaH 809 has a CRE age of ~5.4 Ma, which falls into the typical range of exposure ages for ureilites; the angrite NWA 12934 has a CRE age of ~49 Ma, which is within the main range of exposure ages reported for angrites (0.2–56 Ma). We calculate a CRE age of ~2.4 Ma for the brachinite NWA 12573, which falls into a possible "cluster" in the brachinite CRE age histogram around ~3 Ma. Three lodranites (NWA 11901, NWA 7474, and NWA 6685) have CRE ages higher than the average CRE ages of lodranites measured so far, NWA 11901 and NWA 6685 having CRE ages far higher than the CRE age already reported by Li et al. (2019) on NWA 8118. The measured ^{40}K-^{40}Ar gas retention ages fit well into established systematics. The gas retention age of Tafassasset is consistent, within respective uncertainties, with that previously calculated by Patzer et al. (2003). Our study indicates that Tafassasset originates from a meteoroid with a preatmospheric radius of ~20 cm, however discordant with the radius of ~85 cm inferred in a previous study (Patzer et al., 2003).

INTRODUCTION

Cosmic ray exposure (CRE) ages are useful in establishing histograms in which peaks represent the major collisions in the parent bodies responsible for the ejection of meteorites of each type. The determination of CRE ages not only provides information about the delivery mechanisms of small bodies in the solar system but also helps to identify possible source crater pairing (e.g., Eugster et al., 2006; Herzog & Caffee, 2014; Smith et al., 2021; Stephenson et al., 2017; Zeigler et al., 2005). Gas retention ages based on radiogenic ^{4}He and ^{40}Ar provide valuable information about the thermal and alteration history of meteorites. The combination of both CRE ages and gas retention ages is a good way to determine whether two meteorites are source crater paired (e.g., Eugster et al., 2006; Herzog & Caffee, 2014; Smith et al., 2021; Stephenson et al., 2017). Particularly, CRE age histograms, which represent records of CRE ages for a same meteorite class, are useful to investigate catastrophic impact events in the asteroid belt.

Among meteorites, achondrites consist of silicate-rich igneous rocks that are the result of early large-scale melting processes taking place on a differentiated asteroid (e.g., Jones, 2003; Wadhwa, 2014). Achondrites are further subdivided into (1) "primitive achondrites" including acapulcoites, lodranites, ungrouped primitive achondrites, and (2) other achondrites including winonaites, brachinites, ureilites, angrites, HED (howardites, eucrites, diogenites), aubrites, Martian, and Lunar. Primitive achondrites are defined as meteorites that lost their chondritic texture due to heating or melting but still are characterized by a nearly chondritic composition (e.g., Collinet & Grove, 2020). At the time of writing, 42 angrites, 57 brachinites, 82 winonaites, 192 members of the acapulcoite–lodranite family, 673 ureilites, and 354 primitive achondrites are reported in the Meteoritical Bulletin Database (MBD, as of July 18, 2023, https://www.lpi.usra.edu/meteor/metbull.php). In addition, 144 achondrites are classified as ungrouped/unclassified.

Considering the CRE age data of angrites, it is notable that only scarce data are available to date; Herzog and Caffee (2014) compiled CRE ages of seven, with ages ranging from ~0.2 Ma (but rather uncertain) to ~56 Ma, which would correspond to five ejection events on the angrite parent body. Recently, Wieler et al. (2016) calculated the CRE age of NWA 7812 to be ~20 to 21 Ma, however doubtful due to the presence of SCRs inferred from the cosmogenic (cos) $(^{21}Ne/^{22}Ne)_{cos}$ ratios. The presence of SCRs has implications in CRE age determination, as discussed in, for example, Wieler et al. (2016) or Roth et al. (2017). Wieler et al. (2016) pointed out that taken together, the data for all measured angrites might indicate nine ejection events.

Ureilites remain a mystery for several reasons. Although considered partial melt residues, they have characteristics of chondritic material such as their oxygen isotopic composition or their high noble gas abundances showing a trapped chondritic isotopic composition (e.g., Leya & Stephenson, 2019; Rai et al., 2003). Ureilite progenitors were believed to be ejected from a single impact event on the ureilite parent body (UPB) (Goodrich et al., 2004). The compilation of 28 ^{21}Ne CRE ages in Herzog and Caffee (2014) as well as in the recent study by Leya and Stephenson (2019) indicates that CRE ages span from as young as ~100 ka up to ~50 Ma; notably, four meteorites show extremely young CRE ages <2 Ma (Herzog & Caffee, 2014). Altogether, the literature data (Beard & Swindle, 2017; Herzog & Caffee, 2014) and the 10 newly measured ureilites by Leya and Stephenson (2019) consist of 41 CRE ages for ureilites, divided into six clusters which could however not be clearly separated due to uncertainties inherent to CRE age calculations (Beard & Swindle, 2017; Leya & Stephenson, 2019).

Brachinites are olivine-rich achondrites. As mentioned earlier, 57 brachinites are reported to date in the MBD; among them, to our knowledge, ~20 brachinites have been measured for their noble gas concentrations (Herzog & Caffee, 2014 and references therein; Beard, 2018; Beard et al., 2018). Brachinites have CRE ages ranging from ~9 to 66 Ma (Beard, 2018). Several peaks are identified in the CRE age histogram of brachinites, leading to the identification of at least six impact events on the brachinite parent body, centered at ~10 Ma, ~15 Ma, ~22–26 Ma, ~40 Ma, ~50 Ma, and ~62–66 Ma (Beard, 2018).

Acapulcoites and lodranites are often regrouped as a single clan referred to as the "acapulcoite–lodranite clan" (hereafter ALC). They are characterized by the presence of highly metamorphosed to partially molten chondritic lithologies (e.g., Keil & McCoy, 2018; Li et al., 2018; Patzer et al., 2004). Based on their mineralogy, chemical composition, isotopic properties, and CRE ages, meteorites from the ALC are believed to originate from the same asteroid parent body; in addition, with CRE ages ranging between 4 and 6 Ma, meteorites from the ALC might have been produced in a single ejection event (Patzer et al., 2004). An exception is Queen Alexandra Range (QUE) 93148, with a reported CRE age of ~14.5 to 15.5 Ma (Weigel et al., 1997). In addition, Herzog and Caffee (2014) point out that CRE ages of meteorites from the ALC are challenging to interpret, because of (1) the observed presence of metal in the coarse-grained structure of, for example, lodranites; (2) high $(^{22}Ne/^{21}Ne)_{cos}$ which might reflect a shallow location on the asteroid parent body, and therefore the likelihood of the presence of SCR-produced noble gases. The presence of SCRs would affect the CRE age determination due to the complexity of

TABLE 1. Description of the meteorites studied in this work: meteorite group, date of collection, total known weight, and CRE age when available from literature.

Meteorite name	Classification	References	Date of collection	Total known weight (kg)	CRE age (Ma)
NWA 12934	Angrite	Gattacceca et al. (2020b)	2018	0.563	—
NWA 12573	Brachinite	Gattacceca et al. (2020b)	2018	0.181	—
JaH 809	Ureilite	Ruzicka et al. (2015)	2013, Oman	1.825	—
NWA 11562	Ungrouped achondrite	Gattacceca et al. (2020a)	2017	1.361	—
Tafassasset	Primitive achondrite	Bouvier et al. (2017)	2000, Niger	114	76.1 ± 15.2[a]
NWA 11901	Lodranite	Gattacceca et al. (2020a)	2017, Western Sahara	0.662	—
NWA 7474	Lodranite	Ruzicka et al. (2015)	2012	0.348	—
NWA 6685	Lodranite	Ruzicka et al. (2014)	2010	0.524	—
NWA 6484	Lodranite	Garvie (2012)	2010	0.688	—
NWA 2871	Acapulcoite	Connolly Jr. et al. (2006)	2005	3.47	—
Sahara 02029	Winonaite	Russell et al. (2004)	2002	0.088	—

[a]Patzer et al. (2003).

the calculation of the SCRs contribution (Herzog & Caffee, 2014; Roth et al., 2017; Wieler et al., 2016); (3) the choice of dating scheme for the determination of CRE age. Recently, Li et al. (2019) measured noble gases in selected meteorites from the ALC; among them, the meteorite NWA 8118 records a CRE age of 39 ± 12 Ma, so far, the longest CRE age ever reported for ALC meteorites.

Winonaites are primitive achondrites associated with the IAB iron meteorites, with a precursor material possibly related to chondrites (e.g., Hunt et al., 2017; Zeng et al., 2019). Only a few studies have focused on the noble gas isotopic compositions of winonaites (e.g., Eugster & Lorenzetti, 2005; Garrison & Bogard, 1997). Garrison and Bogard (1997) analyzed three winonaites; they calculated CRE ages ranging from ~20 to 78 Ma. Large amounts of trapped heavy noble gases have been identified. The meteorite NWA 1058, a probable winonaite candidate, has a CRE age of 38.9 ± 4.0 Ma (Eugster & Lorenzetti, 2005).

On the MBD, 14 meteorites are reported as "achondrite-prim." One example is Tafassasset, whose characteristics are intermediate between both CR chondrites and primitive achondrites (e.g., Gardner-Vandy et al., 2012; Patzer et al., 2003). Based on the noble gas study of Tafassasset, Patzer et al. (2003) demonstrate that the long exposure age of Tafassasset of 76.1 ± 15.2 Ma is inconclusive with a possible link with CR chondrites, which usually have CRE ages in the range of ~1 to 20 Ma (Herzog & Caffee, 2014). Later, Sanborn et al. (2019) classified Tafassasset as an achondrite with carbonaceous chondrite characteristics. In addition to its CRE age, noble gas concentrations and isotopic ratios measured in Tafassasset are not consistent with a classification as CR chondrite (Patzer et al., 2003) and would point toward a possible link with brachinites, as demonstrated by bulk chemical data and rock properties (Nehru et al., 2003).

The main objectives of this study are to measure the light noble gas concentrations and isotopic ratios (He, Ne, and Ar) of the following meteorites: Tafassasset (unclassified primitive achondrite), NWA 12934 (angrite), NWA 12573 (brachinite), JaH 809 (ureilite), NWA 11562 (ungrouped achondrite), four lodranites (NWA 11901, NWA 7474, NWA 6685, and NWA 6484), NWA 2871 (acapulcoite), and Sahara 02029 (winonaite). A quick description of the meteorites, including their petrologic type, the date of find, and their total known weight, is summarized in Table 1. Most of these meteorites have not yet been studied for noble gas analyses; the exception is Tafassasset, as mentioned earlier (Patzer et al., 2003). We systematically study their noble gas compositions (cosmogenic and radiogenic compositions) and determine their CRE and gas retention ages. We analyze their exposure histories in the context of other meteorites of the same group with known ages. Finally, in the absence of bulk chemical data for all of our studied samples, we estimate the shielding conditions of these samples by using the "shielding parameter," that is, the cosmogenic (index "cos") ratio $(^{22}Ne/^{21}Ne)_{cos}$ to determine the preatmospheric size of the meteoroid and the depth of the sample within the parent meteoroid.

SAMPLES AND ANALYTICAL TECHNIQUES

Information on samples studied in this work are summarized in Table 1 and in the references to the Meteoritical Bulletin therein.

NOBLE GAS MEASUREMENTS

Noble gas measurements were performed at the noble gas laboratory at the Institute of Geology and Geophysics, Chinese Academy of Sciences (IGGCAS), Beijing, China. The noble gas concentrations and isotopic ratios (^{3,4}He, ^{20,21,22}Ne, and ^{36,38,40}Ar) were measured in multicollection mode using the noble gas mass spectrometer Noblesse © from Nu Instruments company. A detailed description of the analytical procedures is available in, for example, Smith et al. (2021). Briefly, bulk samples with masses ranging from ~3.2 to ~5.3 mg were first cleaned with ethanol in an ultrasonic bath, dried, weighted, and then loaded into the laser sample chamber of the noble gas extraction and purification line. Note that the selected samples have small masses since they are more suitable for laser heating extraction than samples with larger masses (~20 to 100 mg), usually preferred for furnace heating extraction and to reduce effect of bulk chemical heterogeneity (e.g., Di Gregorio et al., 2019). The whole system was baked and evacuated for ~3 days at ~120°C to remove adsorbed atmospheric gases.

Before any sample measurements, calibrations were performed using standard gases, which, except He, are of atmospheric composition. The He standard is the "He Standard of Japan" ("HESJ") with a well-calibrated ^{3}He/^{4}He ratio of 20.6 ± 0.1 Ra (Matsuda et al., 2002), where Ra stands for the ^{3}He/^{4}He ratio of air (i.e., Ra = 1.4×10^{-6}). Sensitivities and instrumental mass discriminations have been calculated based on the air measurements carried out at the time when the samples have been analyzed.

Blanks were frequently measured, before and after each sample, using the same extraction procedure as for the samples. Typically, they contribute to less than 1% for He, less than 2% for Ne, and less than 5% for Ar isotopes.

Noble gases have been released by heating the samples in a single extraction step, using a CO_2 laser (10.6 μm wavelength and with a 2–3 mm diameter beam size) for ~30 min in total. The released gases were first cleaned using a series of getters, operating at room temperature and 200°C, to remove all reactive gases which would otherwise compromise the measurements (e.g., CO_2, H_2O, hydrocarbons, etc.; Smith et al., 2021). The He-Ne fraction was separated from the Ar fraction using an activated charcoal trap held at LN_2 temperature for 20 min. Subsequently, the Ne fraction was separated from the remaining He by using a cryogenic cold trap held at 35 K for 10 min. A calibrated fraction of the He gas was then introduced into the mass spectrometer. The Ne fraction was released at 80 K for 30 min and the total gas fraction was then introduced into the mass spectrometer; remaining background gases, especially double-charged $^{40}Ar^{++}$ and $^{44}CO_2^{++}$ interfering at m/e = 20 and m/e = 22, respectively, which would compromise the Ne measurements, were further reduced using a charcoal trap held at LN_2 temperature during the measurement. These contributions are in the range of ~0.1%, making the corrections negligible. Finally, Ar was released at ~150°C for 20 min, and a known fraction of the gas was measured. After the first measurement, second extractions at a slightly higher laser power were systematically performed to ensure that samples were completely degassed. The second extractions contribute generally for ~1% for He, ~10% for Ne, and ~5%–7% for Ar. Second extraction contributions were added to the total amount of He, Ne, and Ar, and the total amount of extracted gases was subsequently corrected for blank. Note that third extractions were performed, but the amount of released gases is in the same range as typical blanks.

Sahara (SAH) 02029 has, among the other investigated samples, the lowest measured He and Ne amounts, that is, for some isotopes approximately two times higher than the blank level. It is as well characterized by the presence of a trapped Ne (^{20}Ne/^{22}Ne = 3.343 ± 0.028), and Ar signatures, with ^{36}Ar/^{38}Ar ratio purely atmospheric or Q (^{36}Ar/^{38}Ar = 5.323 ± 0.412). Such low concentrations combined with isotopic ratios close to atmospheric ratio might indicate that part of the noble gases was lost during the gas purification, or simply completely degassed. Only a fraction of Ne is affected by such a problem, since ^{20}Ne/^{22}Ne = 3.343 ± 0.028, lower than the atmospheric value of ^{20}Ne/^{22}Ne = 9.80. However, correction of the Ne data from air contamination in SAH 02029 is doubtful considering the high measured ^{20}Ne/^{22}Ne ratio which leads to high uncertainties during the partition of the noble gas components. For such reason, we do not discuss any further SAH 02029.

RESULTS

The noble gas abundances and isotopic ratios corrected for blank, interference, and instrumental mass discrimination, but before any component deconvolution, are presented in Table 2.

Helium

We assume that the measured ^{3}He concentrations are all cosmogenic (index "cos"), therefore ^{3}He = ^{3}He$_{cos}$. This assumption is justified by the fact that none of the samples measured by us shows ^{3}He/^{4}He ratios with solar

TABLE 2. Analyzed mass of the studied samples and their He, Ne, and Ar concentrations and isotopic ratios.

Samples	Mass (mg)	^{3}He (10^{-8}cm^{3}STP g^{-1})	^{3}He/^{4}He	^{20}Ne (10^{-8}cm^{3}STP g^{-1})	^{20}Ne/^{22}Ne	^{21}Ne/^{22}Ne	^{38}Ar (10^{-8}cm^{3}STP g^{-1})	^{36}Ar/^{38}Ar	^{40}Ar/^{36}Ar
NWA 12934	3.42	34.46 ± 1.89	0.0158 ± 0.0003	9.020 ± 0.494	0.781 ± 0.001	0.847 ± 0.001	11.18 ± 0.61	0.975 ± 0.076	128 ± 10
NWA 12573	4.32	7.057 ± 0.387	0.00215 ± 0.00055	0.965 ± 0.053	0.788 ± 0.001	0.865 ± 0.001	0.139 ± 0.008	2.072 ± 0.160	2213 ± 171
JaH 809	3.56	0.260 ± 0.014	0.00215 ± 0.00042	2.580 ± 0.141	1.238 ± 0.004	0.851 ± 0.003	1.348 ± 0.074	5.031 ± 0.390	50.01 ± 3.87
NWA 11562	5.29	19.27 ± 1.06	0.194 ± 0.004	4.029 ± 0.299	0.913 ± 0.002	0.856 ± 0.002	19.43 ± 1.06	4.871 ± 0.377	6.427 ± 0.498
Tafassasset	4.40	72.85 ± 3.99	0.051 ± 0.001	11.82 ± 0.88	0.824 ± 0.002	0.928 ± 0.002	0.940 ± 0.052	0.799 ± 0.062	631 ± 49
NWA 11901	3.22	79.35 ± 4.35	0.093 ± 0.002	15.07 ± 1.12	0.838 ± 0.002	0.934 ± 0.002	3.209 ± 0.176	0.871 ± 0.068	79.74 ± 6.18
NWA 7474	3.30	54.20 ± 2.97	0.107 ± 0.002	4.601 ± 0.341	0.829 ± 0.002	0.929 ± 0.002	0.957 ± 0.052	3.175 ± 0.246	292 ± 23
NWA 6685	3.43	54.66 ± 2.99	0.048 ± 0.001	12.12 ± 0.90	0.848 ± 0.002	0.900 ± 0.002	4.027 ± 0.221	0.894 ± 0.069	75.42 ± 5.84
NWA 6484	5.11	6.949 ± 0.381	0.00219 ± 0.00004	1.365 ± 0.101	0.903 ± 0.002	0.832 ± 0.002	7.501 ± 0.411	5.039 ± 0.390	376 ± 29
NWA 2871	5.13	7.112 ± 0.390	0.0048 ± 0.0001	1.712 ± 0.127	0.986 ± 0.002	0.896 ± 0.002	2.487 ± 0.136	4.106 ± 0.318	259 ± 20
Sahara 02029	3.75	0.137 ± 0.008	0.00215 ± 0.00042	0.233 ± 0.0128	3.343 ± 0.028	0.564 ± 0.008	0.423 ± 0.023	5.323 ± 0.412	166 ± 13

Note: Data are corrected for blanks, instrumental mass discrimination, and interferences. Since noble gas mass spectrometers are optimized for isotope ratio measurements, the uncertainties are very often much smaller for isotope ratios than for isotope concentrations.

contribution (confirmed by neon, see below). Indeed, the measured $^{3}He/^{4}He$ ratios are in the range of ~0.00215 to 0.194 for NWA 12573/JaH 809/Sahara 02029 and NWA 11562, respectively, therefore at least approximately five times higher than the solar ratio of $(4.64 \pm 0.09) \times 10^{-4}$ (e.g., Füri et al., 2018).

Neon

The measured $^{20}Ne/^{22}Ne$ ratios vary between ~0.781 and 3.343. Sample Sahara 02029 has the highest ratio, all other samples have $^{20}Ne/^{22}Ne$ ratios ranging from ~0.781 to 1.238 (Table 2); therefore, most of the samples have almost purely cosmogenic signatures, with a minor contribution of a trapped component. Details about the amount of cosmogenic and trapped neon will be further examined in the discussion.

Argon

The measured $^{36}Ar/^{38}Ar$ ratios between ~0.779 and 5.323 are consistent with a variable amount of a trapped component in addition to the pure cosmogenic signal, with a $(^{36}Ar/^{38}Ar)_{cos} = 0.63$ (e.g., Leya et al., 2013). Sample Sahara 02029 has the highest $^{36}Ar/^{38}Ar$ ratio, indiscernible from atmospheric ratio or Q, that is $(^{36}Ar/^{38}Ar) = 5.32$. Sample JaH 809 has a measured ratio of $^{36}Ar/^{38}Ar = 5.031$, therefore indicating it either suffers from major atmospheric contamination or it contains a significant amount of "primordial" noble gases (primordially trapped noble gases of solar-like compositions, e.g., Wieler et al., 2006). The $^{40}Ar/^{36}Ar$ ratios vary from ~6.4 to 2213 for NWA 11562 and NWA 12573, respectively. The high $^{40}Ar/^{36}Ar$ ratio in NWA 12573 might suggest radiogenic ^{40}Ar production from high concentrations of K. In addition, Tafassasset has $^{40}Ar/^{36}Ar$ ~631, that is, more than two times higher than the atmospheric ratio, therefore suggesting the possible presence of radiogenic $^{40}Ar_{rad}$.

DISCUSSION

Trapped Composition: Neon-Three Isotope Plot

The Ne isotopic composition of our samples is discussed based on a neon-three isotope diagram (Figure 1). All uncertainties (1σ) for the samples are smaller than the size of the symbols. Figure 1 shows the Ne isotopic signatures of the following trapped endmembers: terrestrial atmosphere (e.g., Eberhardt et al., 1965), "Ne-ureilite" (Ne-U, Göbel et al., 1978), HL (Ott, 2014), and solar wind (SW, Heber et al., 2009). The cosmogenic ratio is assumed as $(^{20}Ne/^{22}Ne)_{cos} = 0.78$ (here the lowest ratio measured by us). There are two important findings. Most of the samples plot close to the cosmogenic range, therefore showing that the Ne isotopic signature of the samples is dominated by cosmogenic-produced Ne, with only a small amount of trapped Ne. The ureilite JaH 809 has a $^{20}Ne/^{22}Ne$ ratio of ~1.238 ± 0.004, slightly above the pure cosmogenic range. Sample Sahara 02029 has the highest measured ratio with $^{20}Ne/^{22}Ne$ ~3.343, therefore showing a major contribution of trapped Ne. Second, the measured Ne isotopic composition of our samples suggests no significant contribution by SCRs. Indeed, cosmogenic Ne solely produced by irradiation by galactic cosmic rays in meteorites with chemical composition similar to chondritic have $(^{21}Ne/^{22}Ne) \geq 0.8$ (Roth et al., 2017). This is of importance, especially for the calculation of the CRE ages of our samples; indeed, the presence of SCRs would affect the CRE age determination. The presence of SCRs would also influence the use of the cosmogenic $(^{21}Ne/^{22}Ne)_{cos}$ ratio as a "shielding parameter" to estimate the preatmospheric radius of the meteoroids. Hence, this finding implies that the measured He concentrations are a mixture of two components, radiogenic due to the decay of U and Th ($^{4}He_{rad}$), and cosmogenic, with:

$$^{4}He_{meas} = {}^{4}He_{rad} + \left(^{4}He/^{3}He\right)_{cos} \times {}^{3}He_{cos},$$

where $^{4}He_{rad}$ represents the radiogenic $^{4}He_{rad}$ produced in situ from the radioactive decay of U and Th, and $(^{4}He/^{3}He)_{cos}$ the cosmogenic He isotopic ratio.

Component Deconvolution, Thermal History, Production Rates, and Cosmic Ray Exposure Ages

The noble gas abundances and isotopic compositions after component deconvolution are included in Table 3. For each of the studied samples, we report the nature of the endmembers used for the component deconvolution for Ne in the Appendix S1: Table S1. Similarly, the detailed calculation of the noble gas production rates is described in the appendices.

Jiddat al Harasis (JaH) 809 (Ureilite)

The measured $^{4}He/^{3}He$ ratio is very high (~465), which therefore implies a major contribution from non-cosmogenic, assumed to be entirely radiogenic ^{4}He. By assuming that (i) all measured (label "meas") $^{3}He_{meas}$ is cosmogenic ("cos"), that is, $^{3}He_{meas} = {}^{3}He_{cos}$, and (ii) a cosmogenic $^{4}He/^{3}He$ ratio of $(^{4}He/^{3}He)_{cos}$ ~5 (e.g., Eugster & Michel, 1995), one can calculate the amount of radiogenic $^{4}He_{rad}$.

The calculated $^{4}He_{rad}$ is reported in Table 3. The amount of radiogenic $^{4}He_{rad}$ represents ~99% of the measured $^{4}He_{meas}$.

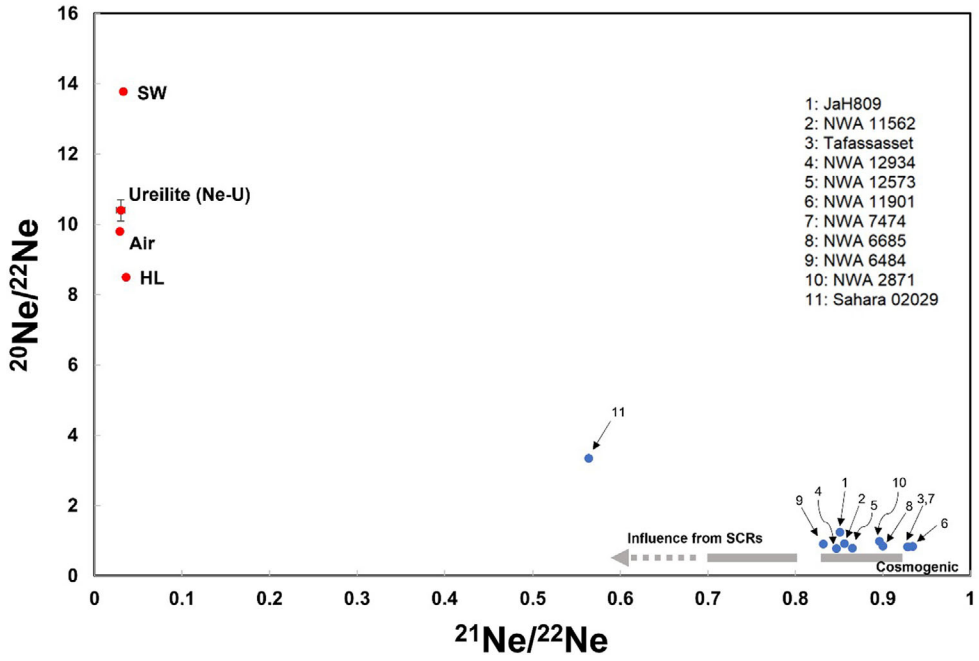

FIGURE 1. Neon three isotope plot for the measured samples. Trapped component endmembers (air, HL, Ne-U, and solar wind—SW) are represented by solid red symbols. Error bars (1SD) are smaller than the size of the symbols and are therefore omitted for clarity. The range of cosmogenic produced by GCRs is calculated for meteoroids with radii of 10–30 cm using an average chemical composition of ordinary chondrites. The potential range of SCRs-produced Ne is highlighted in the plot. It corresponds to cosmogenic $(^{21}Ne/^{22}Ne)_{cos}$ <0.7–0.8, ratios for which the influence of SCRs can only be unequivocal (Roth et al., 2017; Wieler et al., 2016). (Color figure can be viewed at wileyonlinelibrary.com.)

The $^{20}Ne/^{22}Ne$ ratio is ~1.238 ± 0.004, that is, there is a contribution, in addition to cosmogenic, from a trapped component. In the neon-three isotope plot (Figure 1), JaH 809 plots slightly above the cosmogenic endmember range. The Ne endmember compositions for air, SW, HL, as well as ureilite gases (hereafter Ne-U) are also reported, based on the following: $(^{20}Ne/^{22}Ne)_{ureilite}$ = 10.7 (Göbel et al., 1978), and $(^{21}Ne/^{22}Ne)_{ureilite}$ = 0.031 (Göbel et al., 1978); however, the latter is yet poorly constrained (Leya & Stephenson, 2019). After component deconvolution using Ne-U as trapped endmember, the cosmogenic $(^{22}Ne/^{21}Ne)_{cos}$ = 1.128 is well within the range of ratios compiled by Leya and Stephenson (2019), in their Table 4. Based on this ratio, we plot the data for JaH 809 in a "Bern-plot" (Figure 2), that is, $(^{3}He/^{21}Ne)_{cos}$ versus $(^{22}Ne/^{21}Ne)_{cos}$. The sample JaH 809 plots far below both model and empirical regression lines (Leya & Masarik, 2009; Nishiizumi et al., 1980), therefore indicating a major loss of ^{3}H and/or ^{3}He during the cosmic ray exposure history of the meteorite. This agrees with the previous observation by Leya and Stephenson (2019); all ureilites analyzed in their work and most of that compiled from the literature experienced severe loss of ^{3}He (see their fig. 2).

In addition, the ureilite JaH 809 contains resolvable amount of trapped $^{20}Ne_{tr}$. To calculate the amount of trapped $^{20}Ne_{tr}$, we use:

$$^{20}Ne_{tr} = {}^{20}Ne_{m} - {}^{20}Ne_{cos}.$$

By adopting a cosmogenic ratio of $(^{20}Ne/^{22}Ne)_{cos}$ = 0.81, we obtain:

$$^{20}Ne_{tr} = {}^{20}Ne_{m} - 0.81 \times {}^{22}Ne_{cos}.$$

The concentration of cosmogenic $^{22}Ne_{cos}$ is calculated as follows:

$$^{22}Ne_{cos} = {}^{20}Ne_{m} \times \left[1 - \left(^{20}Ne/^{22}Ne\right)_{m} / \left(^{20}Ne/^{22}Ne\right)_{tr}\right] / \left[1 - \left(^{20}Ne/^{22}Ne\right)_{cos} / \left(^{20}Ne/^{22}Ne\right)_{tr}\right]$$

By adopting the following: $(^{20}Ne/^{22}Ne)_{tr}$ = 9.80 (atmospheric ratio), and $(^{20}Ne/^{22}Ne)_{cos}$ ~0.81, we calculate an amount of trapped $^{20}Ne_{tr}$ = (0.616 ± 0.034) × $10^{-8}cm^{3}$ STP g^{-1}, which therefore represents 24% of the total measured $^{20}Ne_{m}$.

The calculated $^{21}Ne_{cos}$ CRE age (T_{21}) is T_{21} = 5.41 ± 0.40 Ma (Table 4), which fits in the range of typical CRE age for ureilites (e.g., Herzog & Caffee, 2014; Leya & Stephenson, 2019). In the latter

TABLE 3. Cosmogenic He, Ne, and Ar concentrations (in 10^{-8} cm^3STP g^{-1}) and isotopic compositions.

Samples	$^3He_{cos} = {}^3He_m$ ($10^{-8}cm^3STP\ g^{-1}$)	^4He_m ($10^{-8}cm^3STP\ g^{-1}$)	$^4He_{rad}$ ($10^{-8}cm^3STP\ g^{-1}$)	$^4He_{rad}$ (%)	$^{21}Ne_{cos}$ ($10^{-8}cm^3STP\ g^{-1}$)	$(^{22}Ne/^{21}Ne)_{cos}$	$^{36}Ar_{cos}$ ($10^{-8}cm^3STP\ g^{-1}$)	$^{38}Ar_{cos}$ ($10^{-8}cm^3STP\ g^{-1}$)	^{40}Ar ($10^{-8}cm^3STP\ g^{-1}$)
NWA 12934	34.46 ± 1.89	2175 ± 119	2002 ± 110	92	9.778 ± 0.725	1.181 ± 0.001	6.940 ± 0.515	10.68 ± 0.79	1435 ± 79
NWA 12573	7.057 ± 0.387	3289 ± 180	3254 ± 178	99	0.846 ± 0.046	1.174 ± 0.001	0.0626 ± 0.0046	0.0963 ± 0.0071	635 ± 34
JaH 809	0.260 ± 0.014	121 ± 7	120 ± 7	99	1.769 ± 0.097	1.128 ± 0.062	0.0543 ± 0.0040	0.0836 ± 0.0062	339 ± 19
NWA 11562	19.27 ± 1.06	99.26 ± 5.44	2.918 ± 0.160	3	3.776 ± 0.207	1.154 ± 0.003	1.214 ± 0.067	1.868 ± 0.102	125 ± 7
Tafassasset	72.85 ± 3.99	1434 ± 79	1069 ± 59	75	13.31 ± 0.73	1.077 ± 0.002	0.592 ± 0.032	0.910 ± 0.049	593 ± 33
NWA 11901	79.35 ± 4.35	857 ± 47	460 ± 25	54	16.79 ± 0.92	1.068 ± 0.002	1.987 ± 0.109	3.057 ± 0.167	256 ± 14
NWA 7474	54.20 ± 2.97	505 ± 28	234 ± 13	46	5.156 ± 0.282	1.075 ± 0.002	0.286 ± 0.016	0.440 ± 0.024	243 ± 13
NWA 6685	54.66 ± 2.99	1149 ± 63	875 ± 48	76	12.86 ± 0.70	1.107 ± 0.002	2.481 ± 0.136	3.817 ± 0.209	304 ± 17
NWA 6484	6.949 ± 0.381	3178 ± 174	3144 ± 172	99	1.257 ± 0.067	1.189 ± 0.003	0.293 ± 0.016	0.451 ± 0.025	2823 ± 155
NWA 2871	7.112 ± 0.390	1483 ± 81	1447 ± 79	98	1.554 ± 0.085	1.093 ± 0.002	0.420 ± 0.023	0.647 ± 0.035	644 ± 35
Sahara 02029	0.137 ± 0.008	63.86 ± 3.50	63.18 ± 3.46	99	0.0385 ± 0.0021	*1.339 ± 0.073*	—	—	375 ± 21

Note: For the component deconvolution, the following assumptions were made (see text): Helium: The measured ^3He is assumed to be entirely cosmogenic, we calculate radiogenic $^4He_{rad}$ by removing cosmogenic ^4He contribution, assuming $(^4He/^3He)_{cos}$ ~5 (Eugster & Michel, 1995). Neon: $(^{20}Ne/^{22}Ne)_{cos}$ as well as the choice of $(^{20}Ne/^{22}Ne)_{tr}$ and $(^{21}Ne/^{22}Ne)_{tr}$ varies for each sample (see text). Argon: we adopt $(^{36}Ar/^{38}Ar)_{tr} = 5.32$, $(^{36}Ar/^{38}Ar)_{cos} = 0.65$. All measured ^{40}Ar is assumed to be purely radiogenic. The given uncertainties (1SD) include the uncertainties for the ion current measurements and uncertainties caused by (i) corrections for interfering isotopes, (ii) corrections for instrumental mass fractionation, and (iii) blank corrections.

Index "cos" stands for cosmogenic, "m" for measured, and "rad" for radiogenic.

Data in italics for cosmogenic $(^{22}Ne/^{21}Ne)cos$ are discarded due to partial loss of noble gas.

TABLE 4. Nominal cosmic ray exposure (CRE) ages (T_3, T_{21}, and T_{38}) of the achondrites based on cosmogenic $^3He_{cos}$, $^{21}Ne_{cos}$, and $^{38}Ar_{cos}$ concentrations, respectively.

Samples	P_3 (10^{-8}cm^{3}STP g^{-1}Ma^{-1})	T_3 (Ma)	P_{21} (10^{-8}cm^{3}STP g^{-1}Ma^{-1})	T_{21} (Ma)	P_{38} (10^{-8}cm^{3}STP g^{-1}Ma^{-1})	T_{38} (Ma)	$T_{adopted}$ (Ma)
NWA 12934	1.53[a]	(22.5 ± 1.7)	0.200[a]	48.9 ± 3.6	0.110[a]	(97.1 ± 7.2)	48.9 ± 3.6
NWA 12573	1.62[b]	(4.36 ± 0.33)	0.352[b]	2.40 ± 0.18	0.0516[c]	(1.87 ± 0.16)	2.40 ± 0.18
JaH 809	Loss of $^3He_{cos}$		0.327[d]	5.41 ± 0.40	—	—	5.41 ± 0.40
NWA 11562	1.63[e]	11.8 ± 0.9	0.178[e]	21.2 ± 1.6	0.144[e]	13.0 ± 1.0	12.4 ± 1.3
Tafassasset	1.84[f]	39.6 ± 5.6	0.269[f]	49.3 ± 5.3	—	—	49.3 ± 5.3
NWA 11901	1.62[e]	(48.9 ± 14.7)	0.140[e]	120.4 ± 36.1	—	—	120.4 ± 36.1
NWA 7474	1.62[e]	33.5 ± 10.0	0.133[e]	38.7 ± 11.6	—	—	36.1 ± 15.3
NWA 6685	1.61[e]	(34.0 ± 10.2)	0.110[e]	116.8 ± 35.1	—	—	116.8 ± 35.1
NWA 6484	1.57[e]	(4.42 ± 1.33)	0.076[e]	16.5 ± 5.0	—	—	16.5 ± 5.0
NWA 2871	1.61[e]	(4.41 ± 3.91)	0.119[e]	13.1 ± 3.9	—	—	13.1 ± 3.9
SAH 02029	—	—	—	—	—	—	—

Note: The production rates P_i for each nuclide i and each meteorite, used for the CRE age calculations, are given. Criteria of selection for the CRE ages are detailed in the text. For clarity, we add parentheses to the CRE ages which are considered doubtful and not taken into account for the average CRE age calculation. Because of the heterogeneity in the distribution of the target elements for the production of ^{38}Ar (i.e., Fe, Ni, and Ca) in lodranites (Weigel et al. 1999), we do not consider ^{38}Ar production rate and hence do not calculate T38.

[a]Wieler et al. (2016).

[b]Based on production rates in Patzer et al. (2003).

[c]Based on the average chemistry of Brachina and on the production rates given by Beard and Swindle, (2017).

[d]Leya and Stephenson (2019).

[e]Based on the empirical relation between $P_{3,21,38}$ and $(^{22}Ne/^{21}Ne)_{cos}$ (Eugster & Michel, 1995).

[f]Based on a Tafassasset chemical composition available in Gardner-Vandy et al. (2012), on the shielding indicator $(^{22}Ne/^{21}Ne)_{cos}$, and on the empirical relations by Eugster and Michel (1995).

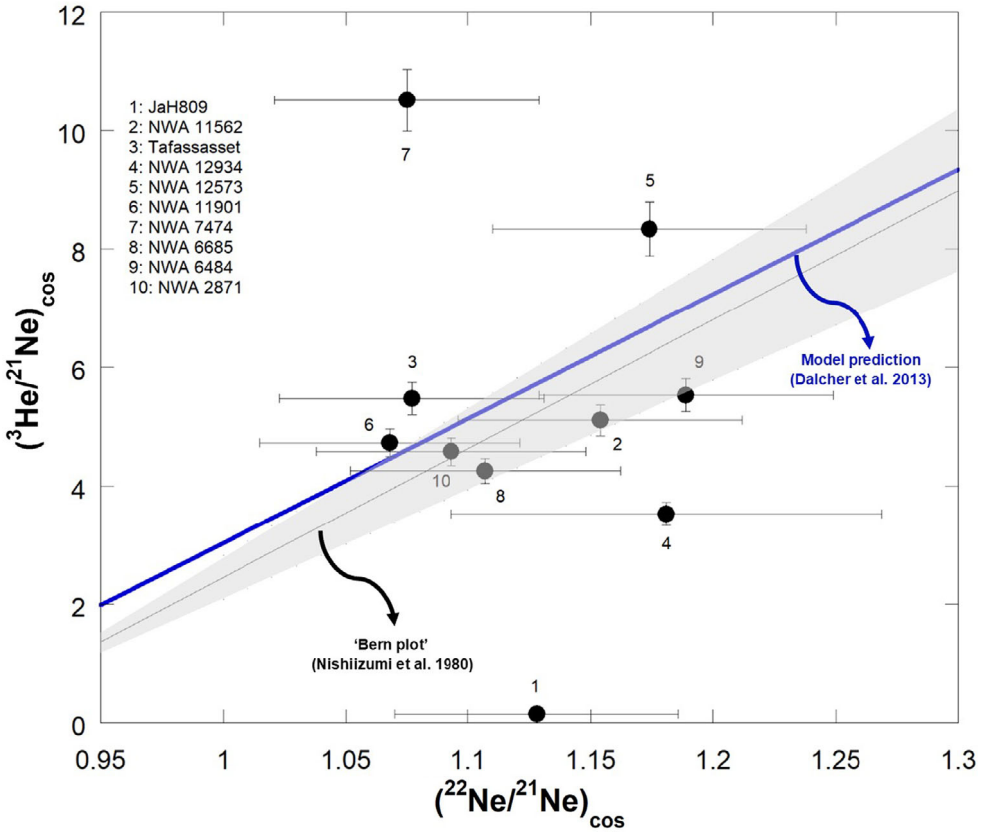

FIGURE 2. Cosmogenic $^3He/^{21}Ne$ versus $^{22}Ne/^{21}Ne$ (so-called "Bern plot"). The data for the 10 measured samples are reported here, as well as the empirical correlation for chondrites given by Nishiizumi et al. (1980), shown here in black. The gray shaded area represents the ±15% uncertainties envelope from that correlation. The best-fit line through model predictions for ordinary chondrites from Dalcher et al. (2013) is shown in blue. Error bars are 1SD. (Color figure can be viewed at wileyonlinelibrary.com.)

study, Leya and Stephenson (2019) pointed out that 11 of their 40 studied ureilites have CRE ages ≤5.8 Ma, some having extremely low CRE ages (ALHA78019 has a CRE age of 0.560 Ma) However, the CRE age histogram for ureilites spreads over a range of 40–45 Ma, usually showing a decrease in number for greater CRE ages. Recently, noble gases have been measured in 18 Almahata Sitta samples (Riebe et al., 2022). Similarly, Riebe et al. (2022) used the average ureilite chemical composition of Leya and Stephenson (2019) for the calculation of noble gas production rates. Samples show CRE ages ranging between ~7 and 20 Ma, with most of the samples having CRE ages between ~15 and 20 Ma (Riebe et al., 2022). A comparison between previously published CRE ages is ambiguous due to the use of different production rate systematics (see Leya & Stephenson, 2019 for details).

Tafassasset (Ungrouped)

Almost ~76% of the total ^4He is radiogenic. Our measured $^{20}Ne/^{22}Ne$ ratio is 0.824 ± 0.002, that is, purely cosmogenic. Hence, the measured ratio and the cosmogenic ratio are identical, that is, $(^{22}Ne/^{21}Ne)_{cos}$ = 1.077 ± 0.054, slightly higher than $(^{22}Ne/^{21}Ne)_{cos}$ ~1.047 ± 0.209 determined by Patzer et al. (2003). On the plot $(^3He/^{21}Ne)_{cos}$ versus $(^{22}Ne/^{21}Ne)_{cos}$ (Figure 2), Tafassasset plots slightly above the empirical and model correlation lines, indicating no or only little noble gas loss. The light noble gas concentrations determined by us are ~6.8%, ~27%, and ~56% lower than those determined by Patzer et al. (2003) for $^3He_{cos}$, $^{21}Ne_{cos}$, and $^{38}Ar_{cos}$, respectively. Such differences can be explained by differences in shielding conditions, discussed in the section "preatmospheric size" hereafter.

We calculate $P_3 = (184 \pm 2) \times 10^{-10} cm^3STP\ g^{-1}\ Ma^{-1}$ and $P_{21} = (27 \pm 1) \times 10^{-10} cm^3STP\ g^{-1}\ Ma^{-1}$ (Table 4). Using these production rates, we calculate CRE ages of T_3 ~40 Ma and T_{21} ~49 Ma. Considering the individual uncertainties in the chemical composition of the samples as well as on the cosmogenic $(^{22}Ne/^{21}Ne)_{cos}$ ratio and production rates, the estimated uncertainty on the CRE ages is ~10%–15%; the thus calculated CRE age $T_{adopted} = T_{21}$ is smaller but still consistent with the CRE age calculated by Patzer et al. (2003).

NWA 12934 (Angrite)

About ~92% of the total measured ^{4}He is radiogenic. With a $^{20}Ne/^{22}Ne = 0.781 \pm 0.001$, the measured $^{21}Ne_{meas}$ is purely cosmogenic. With a $^{36}Ar/^{38}Ar$ ratio of 0.975 ± 0.076, cosmogenic $^{38}Ar_{cos}$ was calculated using a simple two-component deconvolution, based on a mixture between trapped (air) and cosmogenic gases and the following assumptions: $(^{36}Ar/^{38}Ar)_{tr} = 5.32$ and $(^{36}Ar/^{38}Ar)_{cos} = 0.63$.

We calculate nominal CRE ages of: $T_3 = 22.5 \pm 1.7$ Ma, $T_{21} = 48.9 \pm 3.6$ Ma, and $T_{38} = 97.1 \pm 7.2$ Ma. The CRE age calculated using $^{38}Ar_{cos}$ T_{38} is approximately two times higher than T_{21}, itself being approximately two times higher than T_3. We observe the trend $T_3 < T_{21} < T_{38}$, therefore indicating preferential diffusion losses of ^{3}He (and to some extent possible losses of ^{21}Ne), confirmed on the $(^{3}He/^{21}Ne)_{cos}$ versus $(^{22}Ne/^{21}Ne)_{cos}$ plot (Figure 2). Sample NWA 12934 plots slightly below both empirical and model best-fit lines, indicating gas losses by diffusion during the exposure history of the meteorite. However, T_{38} is discarded, the latter being probably inconsistent due to target element inhomogeneity. Although the CRE ages of angrites range from 0.2 to 56 Ma, most of the measured samples have exposure ages ≤20 Ma (Herzog & Caffee, 2014). If we discard our T_3 and our T_{38}, because ^{3}He being, respectively, lost and ^{38}Ar might be influenced by inhomogeneities in the chemical composition of the sample, we adopt a CRE age of $T_{adopted} = T_{21} = 48.9 \pm 3.6$ Ma, hence not within the main grouping for angrites. However, the CRE age of NWA 12934 is in the same range as that of Angra dos Reis, reported at 55.5 ± 1.2 (Lugmair & Marti, 1977). Based on this observation, it is possible that Angra dos Reis and NWA 12934 are source-crater paired.

NWA 12573 (Brachinite)

The brachinite NWA 12573 has a $^{20}Ne/^{22}Ne = 0.788 \pm 0.001$. Therefore, we can assume that all measured $^{21}Ne_{meas}$ is purely cosmogenic. Northwest Africa 12573 has a $^{36}Ar/^{38}Ar$ ratio of 2.072 ± 0.160, which reflects the mixture between a cosmogenic component and a trapped component. To calculate the amount of cosmogenic Ar, we use similar assumptions as for the angrite NWA 12934.

We calculate $P_{38} = 0.0516 \times 10^{-8} cm^3STP\ g^{-1}\ Ma^{-1}$ (see Appendix S1 and Table 4). The thus calculated T_{38} CRE age is $T_{38} = 1.87 \pm 0.16$ Ma.

Additionally, we calculate production rates $P_3 = 1.62 \times 10^{-8} cm^3STP\ g^{-1}Ma^{-1}$ and $P_{21} = 0.352 \times 10^{-8} cm^3STP\ g^{-1}\ Ma^{-1}$. The corresponding CRE ages are $T_3 = 4.36 \pm 0.33$ Ma, $T_{21} = 2.40 \pm 0.18$ Ma, and $T_{38} = 1.87 \pm 0.16$ Ma. Both ages are discordant, with the trend $T_{38} < T_{21} < T_3$. Similar discordant CRE ages have been reported by Patzer et al. (2003), for example, the brachinite Reid 013. These authors preferred the T_{21} age; doing so, our CRE age of $T_{21} = T_{adopted} = 2.40 \pm 0.18$ Ma falls into a possible "cluster" in the brachinite CRE age histogram around ~3 Ma (Beard et al., 2018).

Ungrouped Achondrite NWA 11562

Unlike the other meteorites measured in this work, the total amount of measured ^{4}He is almost purely cosmogenic (~97%); indeed, the measured ratio $(^{4}He/^{3}He)$ ~5.2, that is, well within the expected range of pure cosmogenic ratios (Eugster & Michel, 1995). Assuming a gas retention age of 4.5 Ga and average U and Th concentrations in achondrites (U = 0.220 ppm; Th = 0.190 ppm), one would expect a radiogenic $^{4}He_{rad}$ $\sim 2.91 \times 10^{-4} cm^3$ STP g^{-1}, therefore almost four orders of magnitude higher than the measured $^{4}He_{rad}$ concentration in NWA 11562. Such a low amount of radiogenic $^{4}He_{rad}$ can be explained by diffusion losses due to solar heating during the transfer time of the meteorite from its parent body to the Earth. The measured $^{20}Ne/^{22}Ne = 0.913 \pm 0.002$ is almost purely cosmogenic, whereas the $^{36}Ar/^{38}Ar$ ratio $= 4.87 \pm 0.38$ indicates a major contribution of a trapped component, the latter being considered to be terrestrial atmosphere. After component deconvolution, $^{38}Ar_{cos} = 1.87 \pm 0.10 \times 10^{-8} cm^3STP\ g^{-1}$.

We calculate respective CRE ages of $T_3 = 11.8 \pm 0.9$ Ma, $T_{21} = 21.2 \pm 1.6$ Ma, and $T_{38} = 13.0 \pm 1.0$ Ma. On the Bern plot (Figure 2), there is no indication of any ^{3}He losses, NWA 11562 plotting within the confidence envelope of the correlation line. However, we discard T_{21}, twice higher as the average of T_3 and T_{38}; this might be partly due to some discrepancies in the ^{21}Ne production rate calculations due to unknown target chemistry. However, chemistry inhomogeneities can only partly explain these differences. Therefore, we consider the nominal CRE age of $T_{adopted} = T_{avg} = 12.4 \pm 1.3$ Ma, taken as the average of T_3 and T_{38}.

Lodranites NWA 11901, NWA 7474, NWA 6685, and NWA 6484

Between ~50% and ~99% of the measured $^{4}He_{meas}$ is radiogenic (respectively, NWA 7474/NWA 11901 and NWA 6484). The measured $^{20}Ne/^{22}Ne$ ratios, in the range of 0.829–0.903, show that the Ne isotopic composition is almost purely cosmogenic, with an average $(^{20}Ne/^{22}Ne)_{cos}$ ~0.85, although NWA 6484 has slightly higher amounts of trapped gases, most likely atmospheric Ne (Figure 1). The cosmogenic concentrations are reported in Table 3. As for Ar, the measured $^{36}Ar/^{38}Ar$ ratios range between 0.871 and 5.039, therefore indicating that a large amount of trapped Ar is present in half of our samples (NWA 6484, NWA 7474). Northwest Africa 6484 has a high $(^{22}Ne/^{21}Ne)_{cos}$ which might reflect a shallow location on the asteroid parent body (Herzog & Caffee, 2014).

Note that NWA 7474 probably suffered from partial $^{21}Ne_{cos}$ degassing during measurement, the data point plots far above the correlation line on the Bern plot (Figure 2). However, we have no clear explanation on the possible origin of such $^{21}Ne_{cos}$ degassing.

Because of the heterogeneity in the distribution of the target elements for the production of $^{3}He_{cos}$ and $^{21}Ne_{cos}$, we apply an uncertainty of 30% on both T_3 and T_{21}. We did not calculate CRE ages based on cosmogenic $^{38}Ar_{cos}$ since the distribution in target elements for the production of $^{38}Ar_{cos}$ is much more heterogeneous (Weigel et al., 1999) and can therefore lead to large uncertainties for the calculation of CRE ages.

The T_3 and T_{21} CRE ages of NWA 11901 are ~49 and ~120 Ma, respectively; NWA 7474 are ~33 and ~39 Ma, respectively; NWA 6685 are ~34 and ~117 Ma, respectively; and NWA 6484 are ~4.4 and ~16 Ma, respectively (Table 4). Note that because of possible major compositional changes and of heterogeneities in the distribution of target elements for the production of $^{3}He_{cos}$ and $^{21}Ne_{cos}$ in the meteorites from the ALC (including NWA 11901, NWA 7474, NWA 6685, NWA 6484, and NWA 2871), we apply an uncertainty of 30% on both T_3 and T_{21}. Two main findings can be drawn. First, all but one $^{3}He_{cos}$ CRE ages are lower than $^{21}Ne_{cos}$ CRE ages, by factors ~2.5 to 3.5. The samples in question (NWA 11901, NWA 6685, and NWA 6484) plot on or close to the best-fit line through model predictions for ordinary chondrites from Dalcher et al. (2013), hence indicating that no or only minor losses of $^{3}He_{cos}$ occurred. For this reason, the CRE ages based on $^{3}He_{cos}$ of the above-mentioned samples are not yet understood and therefore discarded from further discussions and calculations. Second, the CRE age of NWA 6484 is consistent within uncertainties with the average CRE ages of lodranites reported in previous work (e.g., Eugster & Lorenzetti, 2005; Weigel et al., 1999). The other three lodranite samples record high CRE ages, far higher exposure ages than that already reported by Li et al. (2019) on NWA 8118, where T_3 = 37.7 Ma and T_{21} = 39.4 Ma, which were so far higher than any previously reported CRE ages for lodranites. This is of great significance since it extends the range of known CRE ages for lodranites to ~120 Ma (note the large uncertainty of ~30%), therefore implying new impact events on the lodranite parent body (Figure 3).

NWA 2871 (Acapulcoite)

The measured $^{20}Ne/^{22}Ne$ ratio of NWA 2871 is 0.986 ± 0.002, that is, there is, in addition to cosmogenic Ne, a small contribution from a trapped component, here considered to be atmospheric; we calculate a $(^{22}Ne/^{21}Ne)_{cos}$ = 1.093 ± 0.055. In the $(^{3}He/^{21}Ne)_{cos}$ versus $(^{22}Ne/^{21}Ne)_{cos}$ plot, there is no evidence of any gas loss, the data plot exactly on the empirical line, although tailored for ordinary chondrites and not for achondrites. The $^{36}Ar/^{38}Ar$ = 4.11 ± 0.32 confirms the presence of a trapped component.

The CRE ages are T_3 = 4.41 ± 1.32 Ma and T_{21} = 13.05 ± 3.91 Ma, which is consistent within uncertainties with most of the acapulcoites, as reported in Weigel et al. (1999) (see their tab. 13). Similar to the lodranite samples, there are potential heterogeneities in the abundances of the target elements for the production of cosmogenic $^{38}Ar_{cos}$; for this reason, P_{38} and T_{38} are not further considered.

Figure 3 represents the compilation of CRE ages extracted from literature for meteorites from the ALC, ureilites, and angrites (Herzog & Caffee, 2014, and references therein). The meteorites studied in this work are plotted in red, whereas previous data on NWA 8118 appear in blue in Figure 3c (Li et al., 2019). Whereas JaH 809 (ureilite), NWA 12934 (angrite), NWA 6484 (lodranite), and NWA 2871 (acapulcoite) have CRE ages consistent with the range of ages determined in other meteorites of the same group, NWA 7474, NWA 6685, and NWA 11901 have greater CRE ages than any ever reported before; an exception is NWA 8118 measured by Li et al. (2019). This implies that, in addition to the already identified breakup events centered at ~4–10 Ma and ~16 Ma (Herzog & Caffee, 2014, Figure 3c), at least two other impact events for lodranites can be recognized, centered at ~30–40 Ma (NWA 7474 and NWA 8118), and ~100–150 Ma (NWA 6685 and NWA 11901).

Preatmospheric Size

To estimate the preatmospheric size (radii) of our studied meteorites, we use the cosmogenic ratio $(^{22}Ne/^{21}Ne)_{cos}$ as a shielding indicator as described in the model of Leya and Masarik (2009) for ordinary chondrites. In addition, due to the absence of major element composition for the studied samples, we use the chemical compositions as reported in Table S2.

For the brachinite NWA 12573, we infer a preatmospheric radius of less than 10 cm (the model results are available only for objects of at least 10 cm), and a shielding depth of no more than ~1–2 cm below the surface. This finding is, however, quite surprising given that no SCR-derived neon was identified. Taking an average density of 3.55 ± 0.06 g cm^{-3} (Macke et al., 2011), a preatmospheric radius of ~5 cm, and assuming the meteoroid to be spherical, we calculate a preatmospheric mass of ~1.9 kg. Assuming now that an average of $\sim 78.4^{+3.1}_{-3.4}$% of the preatmospheric material is lost by ablation during the atmospheric entry (Alexeev, 2003), the estimated mass is ~0.28 kg, that is,

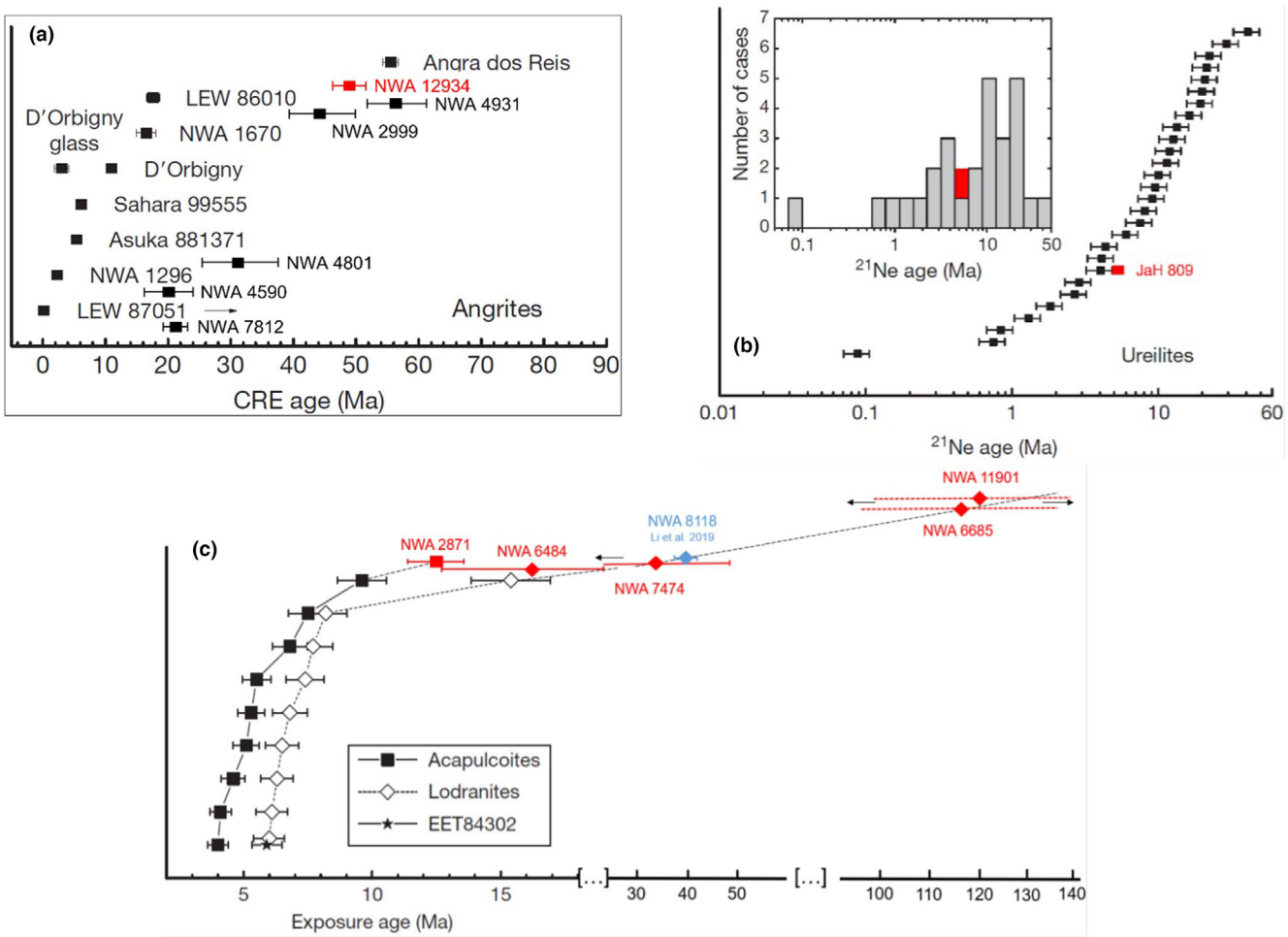

FIGURE 3. Compilation of exposure ages of angrites (a), ureilites (b), and acapulcoites–lodranites (c). The CRE ages of the samples measured by us appear in red. The lodranite NWA 8118 has been measured by Li et al. (2019) and appears as a blue symbol. Reproduced and modified from Herzog and Caffee (2014). Literature data for the CRE ages of angrites: LEW 87051 (Eugster, Michel, & Niedermann, 1991); NWA 1296 (Nakashima et al., 2009); Asuka 881371 (Weigel et al., 1997); Sahara 99555 (Bischoff et al., 2000); D'Orbigny (Kurat et al., 2004); NWA 1670 (Miura et al., 2004); LEW 86010 (Eugster, Beer, et al. 1991, Eugster, Michel, & Niedermann, 1999); Angra dos Reis (Lugmair & Marti, 1977); NWA 7812 (Meier et al., 2013); NWA 4590, NWA 4801, NWA 2999, and NWA 4931 (Nakashima et al., 2018). Literature data for the new CRE ages of acapulcoites–lodranites: NWA 8118 (Li et al., 2019); NWA 6484, NWA 2871, NWA 7474, NWA 6685, and NWA 11901 (this study). No sources provided in Herzog and Caffee (2014) for the literature samples. Literature data include the following samples: for lodranites: Gibson, Y791491, LEW 88280, FRO 90011, GRA 95209, Y74357, Lodran, MAC 88177, and QUE93148; for acapulcoites: ALH 77081, ALH 81261, FRO 95029, GRA 98028, ALH 81187, ALH 84190, Monument Draw, Acapulco, and Y74063 and EET 84302 (acapulcoite/lodranite). (Color figure can be viewed at wileyonlinelibrary.com.)

280 g. The total known weight of NWA 12573 is 181 g, therefore consistent with our calculations.

The calculated cosmogenic ratio $(^{22}Ne/^{21}Ne)_{cos}$ = 1.181 ± 0.088 (Table 3) of the angrite NWA 12934 is consistent with an object having a preatmospheric radius <10 cm.

The lodranite NWA 6484 has a $(^{22}Ne/^{21}Ne)_{cos}$ = 1.189 ± 0.060. However, by considering the average chemical composition of the 24 meteorites data available in Weigel et al. (1999; Table S2), significant variations arise, in particular Na and K, approximately by a factor of 2. The measured ratio is consistent, within its uncertainty, with an object having a preatmospheric radius <10 cm.

The meteorites NWA 11901 and NWA 7474 have $(^{22}Ne/^{21}Ne)_{cos}$ = 1.068 ± 0.053 and $(^{22}Ne/^{21}Ne)_{cos}$ = 1.075 ± 0.054, respectively. Hence, the minimum required radius of the NWA 11901 and NWA 7474 meteoroids is ~20 cm. Using an average bulk density of 3.53 g cm^{-3} (Macke et al., 2011), we calculate for both samples a minimum preatmospheric mass of ~118 kg, which drops to ~18 kg with an ablation loss in the range

of ~85%. This is on average ~27–51 times greater than the total recovered mass; again, these differences can be explained by a stronger ablation during the atmospheric entry.

Using the cosmogenic $(^{22}Ne/^{21}Ne)_{cos}$ = 1.093 ± 0.055 and the average bulk density of acapulcoites as reported in Macke et al. (2011) of 3.42 g cm^{-3}, the minimal preatmospheric radius of the acapulcoite NWA 2871 meteoroid is 20 cm, which would correspond to a preatmospheric mass of ~17 kg, approximately five times higher than the recovered mass of NWA 2871 (3.47 kg).

With an intermediate $(^{22}Ne/^{21}Ne)_{cos}$ = 1.107 ± 0.055, NWA 6685 might originate from a meteoroid with a radius of at least 20 cm, with a shielding depth of ~5 cm. With a calculated preatmospheric mass of ~18 kg (using an average bulk density of 3.53 g cm^{-3}, Macke et al., 2011, and considering an ablation loss in the range of 80%, Alexeev, 2003), we fail to reproduce the total recovered mass of 0.524 kg (Table 1). This discrepancy can be explained by a stronger ablation during the atmospheric entry (overall, literature data indicate ablation losses in the range of 35 ± 12%–100%), and to a minor extent by a wrong assumption in the target element composition of NWA 6685.

Due to the absence of major element composition of NWA 11562 (ungrouped), the preatmospheric size and mass of its meteoroid are not determined.

The ureilite JaH 809 has an intermediate cosmogenic ratio $(^{22}Ne/^{21}Ne)_{cos}$ = 1.128 ± 0.062, consistent with an object having a minimum possible preatmospheric radius of 10 cm, and a shielding depth of ~8 to 10 cm; hence, a deep location of our samples within a small object. With an average density of 3.35 g cm^{-3} (Macke et al., 2011), we estimate a total mass of 2.10 kg whereas the recovered mass (without considering ablation losses) is 1.825 kg (Table 1).

Due to its low $(^{22}Ne/^{21}Ne)_{cos}$ ratio (1.077 ± 0.054), Tafassasset can be considered as part of a big meteoroid. Indeed, low $(^{22}Ne/^{21}Ne)_{cos}$ ratios indicate objects located deep within their meteoroid parent body. Similarly, Patzer et al. (2003) calculated a $(^{22}Ne/^{21}Ne)_{cos}$ ~1.047 and estimated the preatmospheric radius to be in the range of 85 cm (Patzer et al., 2003). Our measured cosmogenic $(^{22}Ne/^{21}Ne)_{cos}$ ratio requires, at least, a preatmospheric radius of 20 cm and an object located at a depth of ~16 to 17 cm (Leya & Masarik, 2009). However, when considering the recovered mass of Tafassasset of 114 kg (Bouvier et al., 2017), an average density of 3.30 g cm^{-3}, and an ablation loss in the range of 80% (Alexeev, 2003), the minimal required radius of the Tafassasset meteoroid is ~40 cm, with a shielding depth of ~11 to 12 cm. However, we only consider here an average ablation loss of ~80%, as determined by Alexeev (2003); with a wider range (from 35 ± 12% to almost 100% of ablation), the preatmospheric radius of Tafassasset, after considering ablation losses, might be as low as ~23 ± 2 cm.

Patzer et al. (2003) estimated a preatmospheric radius in the range of 85 cm for their CRE age calculation. However, with a density of 3.3 g cm^{-3} and assuming the meteoroid has a spherical shape, we calculate, based on the estimated radius of Patzer et al. (2003), a preatmospheric mass of ~8.5 t, whereas the total known recovered mass is estimated to be 114 kg (Bouvier et al., 2017). Assuming that the calculated recovered mass would only account for ~20% of the estimated preatmospheric mass of the Tafassasset meteoroid based on ablation losses of ~80% (Alexeev, 2003), the recovered mass should therefore be in the range of ~1.3 t, which is one order of magnitude higher than the effective collected mass.

For most of the meteorites studied in this work, we observe strong ablation losses occurring during the atmospheric entry. These losses are therefore consistent with previous observations; literature data indicate ablation losses in the range of 35 ± 12%–100%, with average of $78.4^{+3.1}_{-3.4}$% (Alexeev, 2003). However, the preatmospheric masses and radius are only nominal since uncertainties remain on the exact effect of ablation loss for each sample.

Radiogenic Gas Retention Ages

Gas retention ages are calculated using the radiogenic $^{4}He_{rad}$ and $^{40}Ar_{rad}$ concentrations in combination with the abundances in ^{238}U ($T_{1/2}$ = 4.468 × 10^{9} years), ^{235}U ($T_{1/2}$ = 7.038 × 10^{8} years), and ^{232}Th ($T_{1/2}$ = 1.405 × 10^{10} years), parent isotopes of $^{4}He_{rad}$ (^{147}Sm is here omitted, since production from ^{147}Sm is usually only important in the mineral apatite), and ^{40}K in the case of $^{40}Ar_{rad}$. In the absence of U, Th, and K data in our samples, typical concentrations from meteorites of a similar group available in the literature are used. We briefly discuss in the appendices the abundances used for the different samples, which are as well summarized in Table S3.

Before discussing in more detail the gas retention ages, we briefly evoke the caveats of the calculation which need to be considered. First, for all samples, we assume that all ^{40}Ar is radiogenic. Second, as mentioned, we do not have the exact bulk chemical composition of our samples; therefore, we use U, Th, and K data from the literature, when available. Consequently, the gas retention ages calculated here should be considered with great caution and can only represent "nominal" ages.

We calculate the nominal gas retention ages by using the concentrations in radiogenic $^{4}He_{rad}$ and $^{40}Ar_{rad}$ as reported in Table 3, and the adopted U, Th, and K

TABLE 5. Gas retention ages for the measured samples; T_4 stands for ^{4}He retention ages, and T_{40} stands for ^{40}Ar retention ages. All measured ^{40}Ar is assumed to be purely radiogenic.

Samples	$^4He_{rad}$ ($10^{-8}cm^3STP\ g^{-1}$)	T_4 (Ga)	$^{40}Ar_{rad}$ ($10^{-8}cm^3STP\ g^{-1}$)	T_{40} (Ga)
NWA 12934	2002 ± 110	1.16 ± 0.13	1435 ± 79	4.36 ± 0.50
NWA 12573	3254 ± 178	1.13 ± 0.13	635 ± 34	2.23 ± 0.25
JaH 809	120 ± 7	3.88 ± 0.45	339 ± 19	2.21 ± 0.25
NWA 11562	2.918 ± 0.160	0.00998 ± 0.00642	125 ± 7	0.90 ± 0.53
Tafassasset	1069 ± 59	2.54 ± 1.33	593 ± 33	2.4 ± 1.1
NWA 11901	460 ± 25	0.142 ± 0.043	256 ± 14	0.478 ± 0.048
NWA 7474	234 ± 13	0.073 ± 0.022	243 ± 13	0.456 ± 0.046
NWA 6685	875 ± 48	0.268 ± 0.080	304 ± 17	0.550 ± 0.055
NWA 6484	3144 ± 172	0.910 ± 0.273	2823 ± 155	2.65 ± 0.27
NWA 2871	1447 ± 79	0.436 ± 0.131	644 ± 35	1.023 ± 0.102
SAH 02029	63.18 ± 3.46	0.0197 ± 0.0059	375 ± 21	0.663 ± 0.066

Note: The given uncertainties on both T_4 and T_{40} are 1SD. The uncertainties on the gas retention ages for the meteorites of the ALC are taken as ~30% for T_4 and ~10% for T_{40}; they correspond to the individual uncertainties on U, Th, and K, respectively, as stated in Patzer et al. (2003; see text for details).

concentrations for each of our studied samples (appendices and Table S3). The results are reported in Table 5. The calculated ^{4}He (T_4) and ^{40}Ar (T_{40}) retention ages are between 10 Ma and 3.9 Ga for T_4, and between 0.5 and 4.4 Ga for T_{40}. Going into detail, NWA 11562 has the shortest retention age among the investigated meteorites; the calculated T_4 and T_{40} retention ages for this meteorite range between ~10 Ma and ~0.9 Ga, respectively, that is, a difference of a factor of ~100. Note however the high uncertainties due to the range of concentrations in U, Th, and K used for the gas retention age calculations. Such difference between T_4 and T_{40} in sample NWA 11562 can be explained by a preferential diffusion loss of $^4He_{rad}$ compared to $^{40}Ar_{rad}$. Such severe loss of radiogenic gases could be explained by a collision event on the parent asteroid or can be due to solar heating resulting from smaller heliocentric distances before NWA 11562 reached the Earth. However, this hypothesis is not consistent with NWA 11562 having T_3 and T_{38} CRE ages in agreement within their respective uncertainties; the loss of radiogenic $^4He_{rad}$ in NWA 11562 might therefore be explained by a collision event on its parent asteroid.

Regarding the other samples, a similar trend $T_4 < T_{40}$ can be observed, suggesting again a preferential diffusive loss of radiogenic ^{4}He relative to ^{40}Ar. The gas retention ages based on ^{4}He are approximately two times, approximately three times, approximately four times, and approximately six times smaller than T_{40} for NWA 12573/NWA 6685/NWA 2871, for NWA 11901/NWA 6484, for NWA 12934, and for NWA 7474, respectively. The two exceptions are (1) JaH 809 for which $T_4 > T_{40}$ (by a factor of ~1.8); such trend can be explained by an underestimation of the amount of U and Th or an overestimation of the amount of K in our sample. We adjust U and Th concentrations by estimating $T_4 = T_{40}$. Although being a difficult exercise, since either or both U and Th could be underestimated in our first assumption, we find that U and Th should be increased by a factor of ~2.5, assuming both of our estimated U and Th were underestimated. Therefore, this remains consistent with the initial U/Th ratio and with the U/Th ratio range of ureilites; and (2) SAH 02029, for which the calculated T_4 age is the second lowest retention age among the investigated meteorites, consistent with a major loss of noble gases before or during analysis, as mentioned earlier.

Figure 4 represents the ratio of the cosmogenic $^3He_{cos}$ and $^{21}Ne_{cos}$ exposure ages T_3/T_{21} versus the ratio of the gas retention ages T_4/T_{40}. Assuming equal fractional losses of $^3He_{cos}$ and $^4He_{rad}$ and $^{21}Ne_{cos}$ and $^{40}Ar_{rad}$, such plot is useful to assess if any loss of radiogenic gasses occurred before or during the exposure history of our meteorites. All the samples plot above the 1:1 correlation line, indicating for both that a loss of radiogenic $^4He_{rad}$ occurred before their exposure to cosmic rays, as well as ^{3}He diffusive losses. Two exceptions are NWA 12573 and NWA 7474, for which we observe $T_3 > T_{21}$. Such an unusual trend might be explained by an underestimation of the cosmogenic ^{3}He production rate (Dalcher et al., 2013). Samples Tafassasset, NWA 6484, and NWA 11901 are characterized by $T_3 < T_{21}$, but plot within the uncertainty lines (dashed lines, Figure 4), therefore indicating no or only minor diffusion losses. For all samples except JaH 809 (see above), we notice a preferential loss of radiogenic $^4He_{rad}$ during the CRE age of the meteoroid. This trend is particularly clear in Figure 5, which represents the nominal ^{4}He gas retention age versus the nominal ^{40}Ar retention age. From this

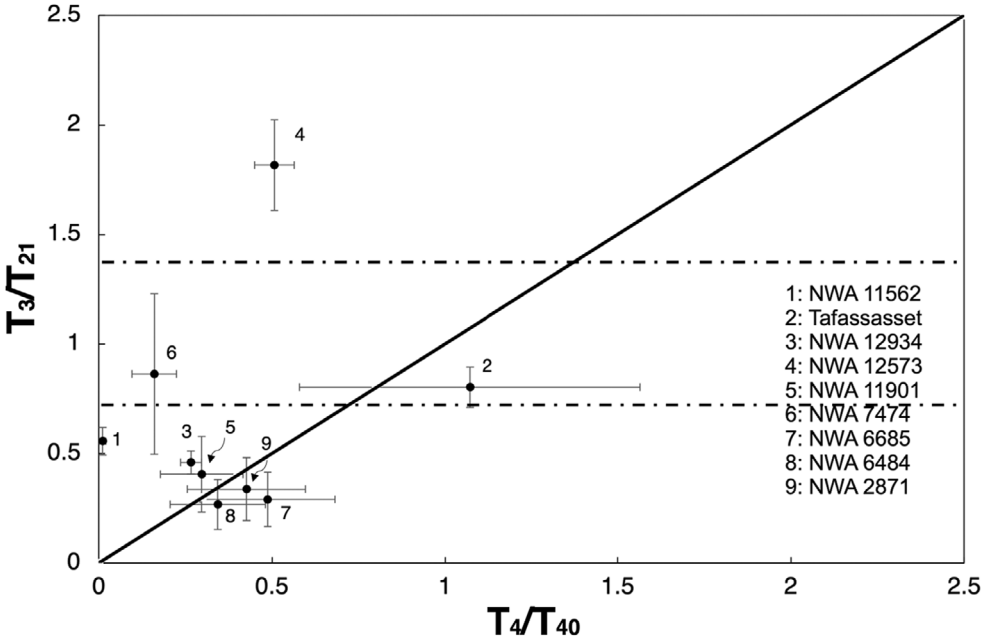

FIGURE 4. Ratio of exposure ages T_3/T_{21} versus ratio of gas retention ages T_4/T_{40}. Meteorites plotting on the solid line with slope 1 indicate no loss of ^{3}He and ^{4}He during their CRE age. Meteorites lying to the left of the solid line (i.e., NWA 12934, NWA 11562) lost radiogenic $^4He_{rad}$ during their exposure history, either at or before breakup of their parent body. Data plotting in-between the horizontal uncertainty dashed lines (i.e., Tafassasset, NWA 7474) show no or only minor indications of ^{3}He and/or ^{3}H diffusive losses. Error bars are 1SD.

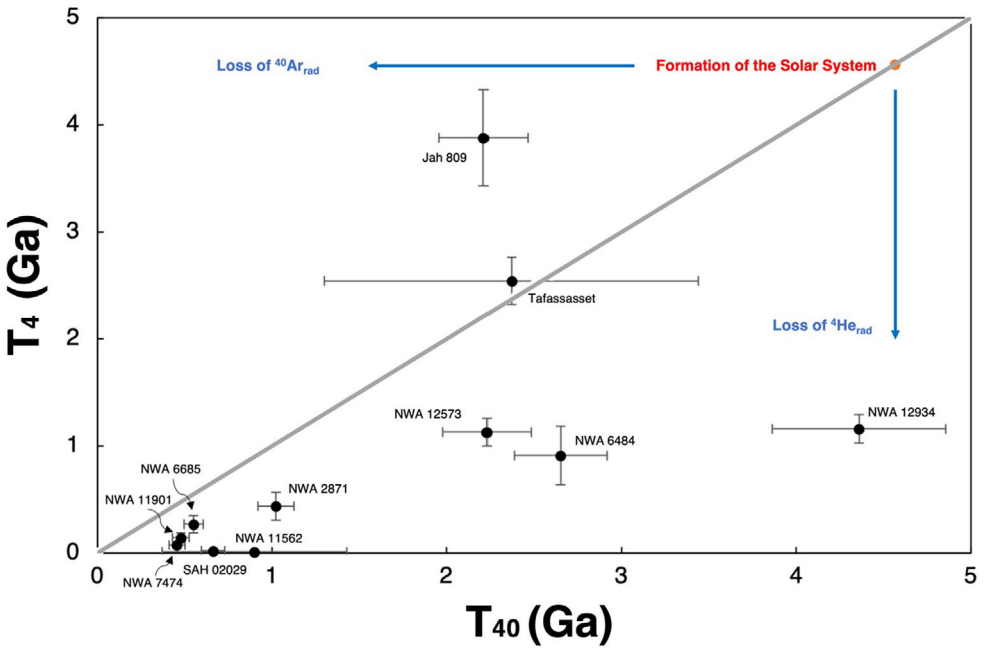

FIGURE 5. Nominal ^{4}He retention age (T_4) versus ^{40}Ar retention age (T_{40}). The 1:1 correlation line appears in bold. Almost all meteorites studied in this show lower nominal T_4 compared to T_{40}. The only exception is JaH 809 with the trend $T_4 > T_{40}$, which could be explained either by an underestimation of the amount of U and Th in the sample, or by more abundant He in the sample. Error bars are 1SD. (Color figure can be viewed at wileyonlinelibrary.com.)

plot, it appears clear that except JaH 809 (see above), all samples have preferentially lost radiogenic $^4He_{rad}$ rather than $^{40}Ar_{rad}$.

Given the preferential diffusive losses of ^{4}He relative to ^{40}Ar, we, therefore, consider the ^{40}K-^{40}Ar gas as preferred retention ages. We now compare our results

with the literature values. The gas retention ages of Tafassasset were previously calculated by Patzer et al. (2003), they found T_4 = 2.09 Ga and T_{40} = 4.33 Ga (see their tab. 2). Our $^4He_{rad}$ age is consistent with that calculated by Patzer et al. (2003), whereas our $^{40}Ar_{rad}$ age is slightly younger than that reported in Patzer et al. (2003), by an almost similar factor of ~1.7 (T_4 = 2.54 Ga). Given an ~20% error on the data of Patzer et al. (2003; as assumed by these authors), and given the large uncertainties of our calculated retention age, the two retention ages T_{40} match well within their respective uncertainties; similarly, retention ages based on radiogenic $^4He_{rad}$ are consistent with each other, both lower than T_{40} and indicating a preferential loss of radiogenic $^4He_{rad}$ in the sample.

Regarding the other meteorite samples studied in this work, they have not been measured for their noble gas records elsewhere to our knowledge. In addition, there are relatively few studies dealing with retention ages of achondrites, and in our case, on angrites, brachinites, ALC, or ureilites. As mentioned in Beard (2018), this is primarily explained by the too scarce or even the lack of major and trace element studies on those samples. We note as well a wide range of concentrations in U, Th, or K for the different aliquots of the same meteorite (see here in the case of Tafassasset meteorite), therefore representing a serious challenge toward a precise determination of their gas retention ages, leading to increase the uncertainties. In the best-case scenario, we could only provide a range of gas retention ages, using the minimum and maximum concentrations in U/Th and K.

CONCLUSIONS

We measured light noble gas in 11 achondrites, the main findings are:

- Noble gas signatures can be explained by a binary mixture between a cosmogenic component and terrestrial atmosphere. There is no evidence of any SCR contributions.
- Two samples, NWA 12934 (angrite) and JaH 809 (ureilite), show strong depletion in ^{3}He, attributed to diffusion losses occurring during the exposure histories of the meteorites. We estimate the loss to be in the range of ~40% for NWA 12934; almost all ^{3}He has been lost in JaH 809. This is, however, rather surprising given that we calculated a retention age of T_4 = 3.9 ± 0.5 Ga; it therefore appears that $^4He_{rad}$ is almost fully retained from U/Th-rich phases whereas ^{3}He, carried in all major phases, appears to have been lost. We currently have no explanation for such trend.
- SAH 02029 lost most of its noble gases during or prior to analysis; the $^{36}Ar/^{38}Ar$ ratio is indistinguishable from air signature ($^{36}Ar/^{38}Ar$ = 5.32 ± 0.41).
- With a CRE age of 49.3 ± 5.3 Ma (Table 4), Tafassasset has a CRE age about ~36% lower than the previous value of 76.1 ± 15.2 Ma (Patzer et al., 2003). However, considering the (large) uncertainties of ~20% adopted by Patzer et al. (2003) and the apparent chemical heterogeneities in the target elements for the production of cosmogenic noble gases, the calculated CRE ages of Tafassasset should only be regarded with caution.
- The adopted CRE ages of lodranites NWA 11901 is ~120 ± 36 Ma, that of NWA 7474 is ~36 ± 15 Ma, that of NWA 6685 is ~117 ± 35 Ma, and that of NWA 6484 is ~16 ± 5 Ma. The latter is consistent, within uncertainties, with the average CRE ages of lodranites. Such high CRE age for lodranite has been already reported by Li et al. (2019) on NWA 8118 (39 ± 12 Ma). This implies that, in addition to the already identified breakup events on the ALC parent body centered at ~4–10 Ma and ~16 Ma (Herzog & Caffee, 2014, Figure 3c), at least two other impact events can be recognized, centered at ~30–40 Ma (NWA 7474 and NWA 8118), and ~90–150 Ma (NWA 6685 and NWA 11901).
- The ureilite JaH 809 has a nominal CRE age of ~5.4 Ma, which is consistent with the typical range of exposure ages for ureilites; the angrite NWA 12934 has a CRE age of ~49 Ma, in the range of CRE ages of angrites (0.2–56 Ma, Herzog & Caffee, 2014; Nakashima et al., 2018). We calculated a CRE age of ~2.4 Ma for the brachinite NWA 12573, hence consistent with a possible peak in the CRE age histogram of brachinites centered at ~3 Ma. Finally, we adopted a nominal CRE age of ~12.4 ± 1.3 Ma for the ungrouped achondrite NWA 11562.
- Losses of radiogenic $^4He_{rad}$ gases have been identified in almost all samples (Table 5) and could be attributed to either a collision event on the parent asteroid or to solar heating resulting from smaller heliocentric distances of those meteorites when traveling to the Earth. The range of ^{40}Ar gas retention ages measured by us is consistent with the expected range of values for meteorites of the same respective class; our calculated ^{40}Ar gas retention age for Tafassasset is in good agree ment with that reported earlier by Patzer et al. (2003).
- Finally, we estimate the preatmospheric sizes and masses of our studied samples using the shielding depth indicator $(^{22}Ne/^{21}Ne)_{cos}$. We could confirm that Tafassasset originated from a meteoroid with a preatm ospheric radius of ~20–40 cm, far smaller than the ~85 cm inferred in a previous study by Patzer et al. (2003).

Acknowledgments—This work has been supported through the National Key R&D Program of China #2020YFE0202100. Additionally, this work has been supported through the SKL-K201802 funding grant from the State Key Laboratory of Lithospheric Evolution, IGGCAS, Beijing, the strategic priority program of the Chinese Academy of Sciences #XDB41010205, the Civil Aerospace pre-research project #D020302, and the Key Deployment Projects of Chinese Academy of Sciences #ZDRW-KT-2019-5-5. We thank the noble gas laboratory team at IGGCAS for their valuable help and support in the preparation and measurements of the meteorite samples. We also thank G. Herzog and H. Busemann whom both provided detailed and constructive reviews which considerably helped in improving the paper. We thank the associate editor M. Caffee for editorial handling.

Conflict of Interest Statement—The authors declare no conflict of interest.

Data Availability Statement—Data openly available in a public repository that issues datasets with DOIs.

Editorial Handling—Dr. Marc W. Caffee

REFERENCES

Alexeev, V. A. 2003. Meteorite Ablation Evaluated from the Data on the Density of Cosmic-Ray Tracks. *Solar System Research* 38:194–202.

Beard, S. P. 2018. Noble Gas Chronology of Meteorites: Brachinites, Ureilites, and Chelyabinsk. PhD Dissertation, The University of Arizona. 185 p.

Beard, S. P., and Swindle, T. D. 2017. Cosmic-Ray Exposure Ages of Brachinites. 80th Annual Meeting of the Meteoritical Society, abstract #6388.

Beard, S. P., Weimer, D., Busemann, H., Maden, C., and Swindle, T. D. 2018. Ne Cosmic-Ray Exposure Ages of Brachinites and Brachinite-Like Achondrites. 49th Lunar and Planetary Science Conference, abstract #2669.

Bischoff, A., Clayton, R. N., Markl, G., Mayeda, T. K., Palme, H., Schultz, L., Srinivasan, G., Weber, H. W., Weckwerth, G., and Wolf, D. 2000. Mineralogy, Chemistry, Noble Gases and Oxygen- and Magnesium-Isotopic Compositions of the Angrite Sahara 99555. *Meteoritics & Planetary Science* 35: A27.

Bouvier, A., Gattacceca, J., Agee, C., Grossman, J., and Metzler, K. 2017. The Meteoritical Bulletin, No. 104. *Meteoritics & Planetary Science* 52: 2284.

Collinet, M., and Grove, T. L. 2020. Formation of Primitive Achondrites by Partial Melting of Alkali-Undepleted Planetesimals in the Inner Solar System. *Geochimica et Cosmochimica Acta* 277: 358–376.

Connolly, H. C., Jr., Zipfel, J., Grossman, J. N., Folco, L., Smith, C., Jones, R. H., Righter, K., et al. 2006. The Meteoritical Bulletin No. 90, 41, 1383–418.

Dalcher, N., Caffee, M. W., Nishiizumi, K., Welten, K. C., Vogel, N., Wieler, R., and Leya, I. 2013. Calibration of Cosmogenic Noble Gas Production in Ordinary Chondrites Based on ^{36}Cl-^{36}Ar Ages. Part 1: Refined Produced Rate for Cosmogenic ^{21}Ne and ^{38}Ar. *Meteoritics & Planetary Science* 48: 1841–62.

Di Gregorio, M., Busemann, H., Hunt, A. C., Krietsch, D., Schönbächler, M., and Maden, C. 2019. Variable Cosmogenic Argon in L/LL5 Chondrite Knyahinya. 82nd Annual Meeting of the Meteoritical Society 2019, #6384.

Eberhardt, P., Eugster, O., and Marti, K. 1965. A Redetermination of Isotopic Composition of Atmospheric Neon. *Zeitschrift fur Naturforshung Part A—Astrophysik Physik und Physikalishe Chemie A* 20: 623–24.

Eugster, O., Beer, J., Burger, M., Finkel, R. C., Hofmann, H. J., Krähenbühl, U., Michel, T., Synal, H. A., and Wölfli, W. 1991. History of Paired Lunar Meteorites MAC 88104 and MAC 88105 Derived from Noble Gas Isotopes, Radionuclides and Some Chemical Abundances. *Geochimica et Cosmochimica Acta* 55: 3139–48.

Eugster, O., Herzog, G. F., Marti, K., and Caffee, M. W. 2006. Irradiation Records, Cosmic-Ray Exposure Ages, and Transfer Times of Meteorites. In *Meteorites and the Early Solar System II*, edited by D. S. Lauretta, and H. Y. McSween, Jr., 829–851. Tucson, AZ: University of Arizona Press.

Eugster, O., and Lorenzetti, S. 2005. Cosmic-Ray Exposure Ages of Four Acapulcoites and Two Differentiated Achondrites and Evidence for a Two-Layer Structure of the Acapulcoite/Lodranite Parent Asteroid. *Geochimica et Cosmochimica Acta* 69: 2675–85.

Eugster, O., and Michel, T. 1995. Common Asteroid Break-up Events of Eucrites, Diogenites, and Howardites and Cosmic-Ray Production Rates for Noble Gases in Achondrites. *Geochimica et Cosmochimica Acta* 59: 177–199.

Eugster, O., Michel, T., and Niedermann, S. 1991. ^{244}Pu-Xe Formation and Gas Retention Age, Exposure History and Terrestrial Age of Angrites LEW 86010 and LEW 87051: Comparison with Angra dos Reis. *Geochimica et Cosmochimica Acta* 55: 2957–64.

Füri, E., Zimmermann, L., and Saal, A. E. 2018. Apollo 15 Green Glass He-Ne-Ar Signatures-in Search for Indigenous Lunar Noble Gases. *Geochemical Perspective Letters* 8: 1–5.

Gardner-Vandy, K. G., Lauretta, D. S., Greenwood, R. C., McCoy, T. J., Killgore, M., and Franchi, I. 2012. The Tafassasset Primitive Achondrite: Insights into Initial Stages of Planetary Differentiation. *Geochimica et Cosmochimica Acta* 85: 142–159.

Garrison, D. H., and Bogard, D. D. 1997. ^{39}Ar-^{40}Ar Ages and Trapped and Cosmogenic Noble Gases in Winonaite Meteorites. 28th Lunar and Planetary Science, abstract #1099.

Garvie, L. A. J. 2012. The Meteoritical Bulletin, No. 99, April.

Gattacceca, J., McCubbin, F. M., Bouvier, A., and Grossman, J. 2020a. The Meteoritical Bulletin, no. 107.

Gattacceca, J., McCubbin, F. M., Bouvier, A., and Grossman, J. 2020b. The Meteoritical Bulletin, no. 108.

Göbel, R., Ott, U., and Begemann, F. 1978. On Trapped Noble Gases in Ureilites. *Journal of Geophysical Research: Solid Earth* 83: 855–867.

Goodrich, C. A., Scott, E. R. D., and Fioretti, A. M. 2004. Ureilitic Breccias: Clues to the Petrologic Structure and Impact Disruption of the Ureilite Parent Asteroid. *Chemie der Erde* 64: 283–327.

Heber, V. S., Wieler, R., Baur, H., Olinger, C., Friedmann, T. A., and Burnett, D. S. 2009. Noble Gas Composition of the Solar Wind as Collected by the Genesis Mission. *Geochimica et Cosmochimica Acta* 73: 7414–32.

Herzog, G. F., and Caffee, M. W. 2014. Cosmic-Ray Exposure Ages of Meteorites. In *Treatise on Geochemistry*, edited by H. D. Holland, and K. K. Turekian, 2nd ed., vol. 1, 419–453. Oxford: Elsevier.

Hunt, A. C., Benedix, G. K., Hammond, S. J., Bland, P. A., Rehkämper, M., Kreissig, K., and Strekopytov, S. 2017. A Geochemical Study of the Winonaites: Evidence for Limited Partial Melting and Constraints on the Precursor Composition. *Geochimica et Cosmochimica Acta* 199: 13–30.

Jambon, A., Boudouma, O., Fonteilles, M., Le Guillou, C., Badia, D., and Barrat, J.-A. 2008. Petrology and Mineralogy of the Angrite Northwest Africa 1670. *Meteoritics & Planetary Science* 43: 1150–63.

Jones, R. H. 2003. Meteorites. In *Encyclopedia of Physical Science and Technology*, edited by R. A. Meyers, 3rd ed., 559–574. Albuquerque, NM: Academic Press. https://doi.org/10.1016/B0-12-227410-5/00434-8.

Keil, K., and McCoy, T. J. 2018. Acapulcoite-Lodranite Meteorites: Ultramafic Asteroidal Partial Melt Residues. *Geochemistry* 78: 153–203.

Kurat, G., Varela, M. E., Brandstätter, F., Weckwerth, G., Clayton, R. N., Weber, H. W., Schultz, L., Wäsch, E., and Nazarov, M. A. 2004. D'Orbigny: A Non-Igneous Angritic Achondrite? *Geochimica et Cosmochimica Acta* 68: 1901–21.

Leya, I., Ammon, K., Cosarinsky, M., Dalcher, N., Gnos, E., Hofmann, B., and Huber, L. 2013. Light Noble Gases in 12 Meteorites from the Omani Desert, Australia, Mauritania, Canada, and Sweden. *Meteoritics & Planetary Science* 48: 1401–14.

Leya, I., and Masarik, J. 2009. Cosmogenic Nuclides in Stony Meteorites Revisited. *Meteoritics & Planetary Science* 44: 1061–86.

Leya, I., and Stephenson, P. C. 2019. Cosmic Ray Exposure Ages for Ureilites–New Data and a Literature Study. *Meteoritics & Planetary Science* 54: 1512–32.

Li, S., Leya, I., Smith, T., and He, H. 2019. Cosmic-Ray Exposure Ages of Some Primitive Achondrites. 82nd Annual Meeting of the Meteoritical Society, abstract #6174.

Li, S., Yin, Q.-Z., Bao, H., Sanborn, M. E., Irving, A., Ziegler, K., Agee, C., et al. 2018. Evidence for a Multilayered Internal Structure of the Chondritic Acapulcoite-Lodranite Parent Asteroid. *Geochimica et Cosmochimica Acta* 242: 82–101.

Lugmair, G., and Marti, K. 1977. Sm-Nd-Pu Time Pieces in the Angra dos Reis Meteorite. *Earth and Planetary Science Letters* 35: 273–284.

Macke, R. J., Britt, D. T., and Consolmagno, G. J. 2011. Density, Porosity, and Magnetic Susceptibility of Achondritic Meteorites. *Meteoritics & Planetary Science* 46: 311–326.

Matsuda, J., Matsumoto, T., Sumino, H., Nagao, K., Yamamoto, J., Miura, Y., Kaneoka, I., Takahata, N., and Sano, Y. 2002. The $^{3}He/^{4}He$ Ratio of the New Internal He Standard of Japan (HESJ). *Geochemical Journal* 36: 191–95.

Meier, M. M. M., Irving, A. J., and Wieler, R. 2013. Cosmic-Ray Exposure and Gas-Retention Ages of the Unique Quenched Angrite Northwest Africa 7812. *Meteoritics & Planetary Science* 35: 5222.

Meija, J., Coplen, T. B., Berglund, M., Brand, W. A., De Bièvre, P., Gröning, M., Holden, N. E., et al. 2016. IUPAC Technical Report Isotopic Compositions of the Elements 2013 (IUPAC Technical Report). *Pure and Applied Chemistry* 88: 293–306.

Miura, Y. N., Sugiura, N., Kusakabe, M., and Nagao, K. 2004. Noble Gases in Northwest Africa 1670, a New Angrite, and Oxygen Isotopes of this Angrite and some Achondrites. *Antarctic Meteorites* 28: 50–51.

Nakashima, D., Nagao, K., and Irving, A. J. 2009. Noble Gas Retention Ages of Angrites NWA 1296 NWA 2999/4931 NWA 4590 and NWA 4801. *Meteoritics & Planetary Science* 44: 5349.

Nakashima, D., Nagao, K., and Irving, A. J. 2018. Noble Gases in Angrites Northwest Africa 1296, 2999/4931, 4590, and 4801: Evolution History Inferred from Noble Gas Signatures. *Meteoritics & Planetary Science* 53: 952–972.

Nehru, C. E., Prinz, M., Delaney, J. S., Dreibus, G., Palme, H., Spettel, B., and Wänke, H. 1983. Brachina: A New Type of Meteorite, Not a Chassignite. *Journal of Geophysical Research* 88: 237–244.

Nehru, C. E., Weisberg, M. K., Boesenberg, J. S., and Kilgore, M. 2003. Tafassasset: A Metal-Rich Primitive Achondrite with Affinities to Brachinites (abstract #1370). 34th Lunar and Planetary Science Conference, abstract #1370.

Nishiizumi, K., Regnier, S., and Marti, K. 1980. Cosmic Ray Exposure Ages of Chondrites, Pre-Irradiation and Constancy of Cosmic Ray Flux in the Past. *Earth and Planetary Science Letters* 50: 156–170.

Ott, U. 2014. Planetary and Pre-Solar Noble Gases in Meteorites. *Chemie der Erde-Geochemistry* 74: 519–544.

Patzer, A., Hill, D. H., and Boynton, W. V. 2004. Evolution and Classification of Acapulcoites and Lodranites from a Chemical Point of View. *Meteoritics & Planetary Science* 39: 61–85.

Patzer, A., Schultz, L., and Franke, L. 2003. New Noble Gas Data of Primitive and Differentiated Achondrites Including Northwest Africa 011 and Tafassasset. *Meteoritics & Planetary Science* 38: 1485–97.

Rai, V. K., Murty, S. V. S., and Ott, U. 2003. Noble Gases in Ureilites: Cosmogenic, Radiogenic, and Trapped Components. *Geochimica et Cosmochimica Acta* 67: 4435–56.

Riebe, M. E. I., Plant, A., Meier, M. M. M., Will, P., Kramer, A.-K., Bischoff, A., Maden, C., and Busemann, H. 2022. Almahatta Sitta Ureilites-Noble Gases and Cosmic Ray Exposure Ages. 85th Annual Meeting of the Meteoritical Society 2022, abstract #6258.

Roth, A. S. G., Trappitsch, R., Metzler, K., Hofmann, B. A., and Leya, I. 2017. Neon Produced by Solar-Cosmic Rays in Ordinary Chondrites. *Meteoritics & Planetary Science* 52: 1155–72.

Russell, S. S., Folco, L., Grady, M. M., Zolensky, M. E., Jones, R., Righter, K., Zipfel, J., and Grossman, J. N. 2004. The Meteoritical Bulletin, No. 88, July.

Ruzicka, A., Grossman, J., Bouvier, A., Herd, C. D. K., and Agee, C. B. 2015. The Meteoritical Bulletin, No. 102. *Meteoritics & Planetary Science* 50: 1662–1662. https://doi.org/10.1111/maps.12491.

Ruzicka, A., Grossman, J., and Garvie, L. 2014. The Meteoritical Bulletin No. 100.

Sanborn, M. E., Wimpenny, J., Williams, C. D., Yamakawa, A., Amelin, Y., Irving, A. J., and Yin, Q.-Z. 2019. Carbonaceous Achondrites Northwest Africa 6704/6693: Milestones for Early Solar System Chronology and Genealogy. *Geochimica et Cosmochimica Acta* 245: 577–596.

Smith, T., He, H., Li, S., Ranjith, P. M., Su, F., Gattacceca, J., Braucher, R., and ASTER-Team. 2021. Light Noble Gas Records and Cosmic-Ray Exposure Histories of Recent Ordinary Chondrite Falls. *Meteoritics & Planetary Science* 56: 2002–16.

Stephenson, P., Lin, Y., and Leya, I. 2017. The Noble Gas Concentrations of the Martian Meteorites GRV 99027 and Paired NWA 7906/NWA 7907. *Meteoritics & Planetary Science* 52: 2505–20.

Swindle, T. D., Kring, D. A., Burkland, M. K., Hill, D. H., and Boynton, W. V. 1998. Noble Gases, Bulk Chemistry, and Petrography of Olivine-Rich Achondrites Eagles Nest and LEW 88763: Comparison to Brachinites. *Meteoritics & Planetary Science* 33: 31–48.

Wadhwa, M. 2014. Solar System Time Scales from Long-Lived Radioisotopes in Meteorites and Planetary Materials. In *Treatise on Geochemistry*, Vol. 1: Meteorites, Comets, and Planets, edited by H. D. Holland, and K. K. Turekian, 2nd ed., 397–418. Tempe, AZ: Elsevier.

Weigel, A., Eugster, O., Koeberl, C., and Krähenbühl, U. 1997. Differentiated Achondrites Asuka 881371, an Angrite, and Divnoe: Noble Gases, Ages, Chemical Composition, and Relation to Other Meteorites. *Geochimica et Cosmochimica Acta* 61: 239–248.

Weigel, A., Eugster, O., Koeberl, C., Michel, R., Krähenbühl, U., and Neumann, S. 1999. Relationships among Lodranites and Acapulcoites: Noble Gas Isotopic Abundances, Chemical Composition, Cosmic-Ray Exposure Ages, and Solar Cosmic Ray Effects. *Geochimica et Cosmochimica Acta* 63: 175–192.

Wieler, R., Busemann, H., and Franchi, I. A. 2006. In *Trapping and Modification Processes of Noble Gases and Nitrogen in Meteorites and their Parent Bodies. Meteorites and the Early Solar System II*, edited by D. S. Lauretta, and H. Y. McSween, Jr., 499–521. Tucson, AZ: University of Arizona Press.

Wieler, R., Huber, L., Busemann, H., Seiler, S., Leya, I., Maden, C., Masarik, J., et al. 2016. Noble Gases in 18 Martian Meteorites and Angrite Northwest Africa 7812-Exposure Ages, Trapped Gases, and a re-Evaluation of the Evidence for Solar Cosmic Ray-Produced Neon in Shergottites and Other Achondrites. *Meteoritics & Planetary Science* 51: 407–428.

Zeigler, R. A., Korotev, R. L., Jolliff, B. L., and Haskin, L. A. 2005. Petrography and Geochemistry of the LaPaz Icefield Basaltic Lunar Meteorite and Source Crater Pairing with Northwest Africa 032. *Meteoritics & Planetary Science* 40: 1073–1101.

Zeng, X., Shang, Y., Li, S., Li, X., Wang, S., and Li, Y. 2019. The Layered Structure Model for Winonaite Parent Asteroid Implicated by Textural and Mineralogical Diversity. *Earth, Planets and Space* 71: 38.

Zipfel, J., Palme, H., Kennedy, A. K., and Hutcheon, I. D. 1995. Chemical Composition and Origin of the Acapulco Meteorite. *Geochimica et Cosmochimica Acta* 59: 3607–27.

SUPPORTING INFORMATION

Additional supporting information may be found in the online version of this article.

Data S1. Deconvolution endmembers for the calculation of cosmogenic neon.